The Journal of Immunology

T Follicular Regulatory Cell–Derived Fibrinogen-like Protein 2 Regulates Production of Autoantibodies and Induction of Systemic Autoimmunity

Waradon Sungnak, Allon Wagner, Monika S. Kowalczyk, Lloyd Bod, Yoon-Chul Kye, Peter T. Sage, Arlene H. Sharpe, Raymond A. Sobel, Francisco J. Quintana, Orit Rozenblatt-Rosen, Aviv Regev, Chao Wang, Nir Yosef and Vijay K. Kuchroo

J Immunol 2020; 205:3247-3262; Prepublished online 9 November 2020;
doi: 10.4049/jimmunol.2000748
http://www.jimmunol.org/content/205/12/3247

The Journal of Immunology is published twice each month by
The American Association of Immunologists, Inc.,
1451 Rockville Pike, Suite 650, Rockville, MD 20852

Print ISSN: 0022-1767 Online ISSN: 1550-6606.

T Follicular Regulatory Cell–Derived Fibrinogen-like Protein 2 Regulates Production of Autoantibodies and Induction of Systemic Autoimmunity

Waradon Sungnak,* Allon Wagner,† Monika S. Kowalczyk,‡ Lloyd Bod,* Yoon-Chul Kye,* Peter T. Sage,*,§ Arlene H. Sharpe,*,§ Raymond A. Sobel,¶ Francisco J. Quintana,‖ Orit Rozenblatt-Rosen,‡ Aviv Regev,‡ Chao Wang,* Nir Yosef,† and Vijay K. Kuchroo*,‡,‖

T follicular regulatory (TFR) cells limit Ab responses, but the underlying mechanisms remain largely unknown. In this study, we identify Fgl2 as a soluble TFR cell effector molecule through single-cell gene expression profiling. Highly expressed by TFR cells, Fgl2 directly binds to B cells, especially light-zone germinal center B cells, as well as to T follicular helper (TFH) cells, and directly regulates B cells and TFH in a context-dependent and type 2 Ab isotype–specific manner. In TFH cells, Fgl2 induces the expression of Prdm1 and a panel of checkpoint molecules, including PD1, TIM3, LAG3, and TIGIT, resulting in TFH cell dysfunction. Mice deficient in Fgl2 had dysregulated Ab responses at steady-state and upon immunization. In addition, loss of Fgl2 results in expansion of autoreactive B cells upon immunization. Consistent with this observation, aged Fgl2$^{-/-}$ mice spontaneously developed autoimmunity associated with elevated autoantibodies. Thus, Fgl2 is a TFR cell effector molecule that regulates humoral immunity and limits systemic autoimmunity. ***The Journal of Immunology*****, 2020, 205: 3247–3262.**

B cell–mediated Ab production is a major component of adaptive immunity. Multiple processes that contribute to optimal Ab responses depend on a histologically specialized site called the germinal center (GC) located in B cell zones of secondary lymphoid organs. Such processes include B cell affinity maturation, class-switch recombination (CSR), plasma cell differentiation, and memory B cell generation (1, 2). GC formation, maintenance, and Ab class switching depend on help from specialized CD4$^+$ T follicular helper (TFH) cells (3), which were first described as CD4$^+$ T cells expressing a high level of the chemokine receptor CXCR5 that drives TFH migration to B cell follicles in response to the chemokine CXCL13 (4–6). TFH cells express the transcription factor Bcl6, a master regulator that mediates a unique TFH transcriptional program, whereas the transcription factor Blimp1 (encoded by the gene Prdm1) antagonizes Bcl6 and inhibits TFH differentiation and help (7–9). In addition to the expression of Bcl6, TFH cells express transcription factor cMaf, which induces IL-21 production (10) and Ascl2, which is critical for the expression of CXCR5 and trafficking of TFH cells into the GCs (11). TFH cells also express high levels of the costimulatory molecule ICOS and the coinhibitory molecule PD1. These cells provide help to B cells through costimulatory molecules and cytokines, including CD40L, IL-21, and IL-4 (6, 10, 12–18).

Recently, a CXCR5$^+$Foxp3$^+$ CD4 T cell population was shown to mediate inhibitory effects on GC reactions and Ab responses, and thus, the cells were defined as T follicular regulatory (TFR) cells (19–21). Moreover, the cells have been shown to limit autoimmunity responses in animal models of influenza infection and Sjogren disease (22, 23). Unlike TFH cells, however, Bcl6 and Blimp1 are coexpressed in TFR cells. Blimp1 has been previously shown to influence regulatory T (Treg) function by inducing an effector regulatory phenotype (24). It is expressed by Treg at mucosal sites and by a small subset of splenic Treg cells that produce IL-10 in a Blimp1 (25). Similar to these Treg cells, TFR cells share high expression of IL-10, GITR, and ICOS. Thus, TFR cells were suggested to be the follicular counterparts of the Blimp1$^+$IL-10$^+$ effector Treg cells found at mucosal surfaces (25, 26) and, in addition, because of their presence in GCs to regulate T cell–dependent Ab production by B cells. Recent studies suggested that TFR cells are able to durably alter multiple metabolic

*Evergrande Center for Immunologic Diseases, Brigham and Women's Hospital, Harvard Medical School, Boston, MA 02115; †Department of Electrical Engineering and Computer Science, Center for Computational Biology, University of California, Berkeley, CA 94720; ‡Klarman Cell Observatory, Broad Institute of MIT and Harvard, Cambridge, MA 02142; §Department of Microbiology and Immunobiology, Harvard Medical School, Boston, MA 02115; ¶Department of Pathology, Stanford University, Stanford, CA 94305; and ‖Ann Romney Center for Neurologic Diseases, Brigham and Women's Hospital, Boston, MA 02115

ORCIDs: 0000-0001-8124-0863 (L.B.); 0000-0002-0477-9002 (R.A.S.); 0000-0003-3084-6093 (C.W.).

Received for publication July 14, 2020. Accepted for publication October 15, 2020.

This work was supported by the National Institutes of Health/National Institute of Allergy and Infectious Diseases (1AI39671, 2P01AI56299, and 5P01AI129880). Lupus Research Alliance William E. Paul Distinguished Innovator Award 594584 supports work performed in the Kuchroo Lab. C.W. is supported by National Multiple Sclerosis Society Career Transition Fellowship TA-1605-08590.

W.S., C.W., and V.K.K. conceived the project. W.S. and C.W. designed most biological experiments. W.S. performed most experiments, and W.S., L.B., and Y.-C.K. analyzed the data. A.W., L.B., Y.-C.K., and N.Y. performed and devised computational analyses. M.S.K., O.R.-R., and A.R. performed and supervised single-cell RNA sequencing experiments. R.A.S. performed histological analysis. F.J.Q. performed autoantigen microarray. P.T.S. and A.H.S. provided help on experimental methods and provided CD28$^{-/-}$ mice. W.S., A.W., C.W., and V.K.K. wrote the paper with input from all of the authors.

Address correspondence and reprint requests to Prof. Vijay K. Kuchroo, Brigham and Women's Hospital and Harvard Medical School, 60 Fenwood Road, BTM 10016F, Boston, MA 02115. E-mail address: vkuchroo@evergrande.hms.harvard.edu

The online version of this article contains supplemental material.

Abbreviations used in this article: ANA, anti-nuclear Ag; ASC, Ab-secreting cell; CSR, class-switch recombination; GC, germinal center; His-Tag, polyhistidine tag; LZ, light-zone; NP, 4-hydroxy-3-nitrophenylacetyl; nTreg, natural Treg; PP, Peyer's patches; qPCR, quantitative PCR; RNA-seq, RNA sequencing; TFH, T follicular helper; TFR, T follicular regulatory; Treg, regulatory T; *t*-SNE, *t*-distributed stochastic neighbor embedding.

pathways in B cells through epigenetic changes, resulting in their diminished Ab production (27). Expression of the coinhibitory receptor CTLA4 on TFR cells was demonstrated to be important for TFR cell effector functions, as the loss of CTLA4 on TFR cells led to their reduced capacity to suppress Ab responses (28, 29). However, the effector mechanisms used by TFR cells to suppress B cells, dendritic cells or other helper T cells, have not been fully investigated.

We performed population and single-cell RNA sequencing (RNA-seq) assays of $CD4^+$ T cells and computationally analyzed their transcriptome to identify soluble molecules that are differentially expressed in TFR/effector Treg cells in comparison with TFH cells or conventional Treg cells. We identified Fgl2 as a TFR cell effector molecule and a direct regulator of Ab responses. The molecule binds to B cells, particularly light-zone (LZ) GC B cells and TFH cells and thereby directly modulates CSR in B cells and cytokine production from TFH cells. The inhibitory functions of Fgl2 were partly due to its effects on TFH cells, as it induces expression of *Prdm1* and a panel of coinhibitory checkpoint molecules. Fgl2-deficient mice have dysregulated homeostatic and immunization-induced Ag-specific Ab responses. Fgl2-deficient TFR cells failed to suppress IgG1 production in vitro and in vivo. Moreover, aged Fgl2-deficient mice showed signs of autoimmunity with elevated autoantibody level. Together, these findings demonstrate that Fgl2, a TFR effector molecule, regulates TFH cell and B cell functions and loss of Fgl2 results in dysregulated autoantibody responses and development of systemic autoimmunity.

Materials and Methods

Mice

Wild-type CH7 black 6 (C57BL/6J), $Fcgr2b^{-/-}$, $Fcgr3^{-/-}$, and $Prdm1^{fl/fl}$ mice were purchased from The Jackson Laboratory. Foxp3-IRES-GFP and $Fgl2^{-/-}$ mice on the C57BL/6 background have been published previously (30, 31). $Fgl2^{-/-}$ with Foxp3-IRES-GFP reporter mice were bred in the laboratory. $CD28^{-/-}$ mice on the C57BL/6 background were from A. Sharpe laboratory. All mice were between 6 and 8 wk of age at the time of experiments unless specific ages were mentioned in particular experiments. All mice used in each experiment were age matched and gender matched. The experiments were conducted in accordance with animal protocols approved by the Harvard Medical Area Standing Committee on Animals or Brigham and Women's Hospital Institutional Animal Care and Use Committee.

Immunizations

Mice were s.c. immunized with 100 μg 4-hydroxy-3-nitrophenylacetyl (NP)-OVA (Biosearch Technologies) emulsified in CFA (BD Biosciences) in the mouse flanks as previously described (32). For immunization to induce autoreactive B cells, additional heat-killed, dried *Mycobacterium tuberculosis* was added to CFA to the final concentration of 4 mg/ml. Mice were sacrificed later, and inguinal lymph nodes were harvested.

Abs

The following Abs were used for surface staining: anti-CD4 (RM4-5), anti-CD19 (6D5), anti-CXCR5 biotin (2G8), anti-PD1 (RMP1-30), anti-Fas (15A7), GL7 (GL7), anti-IgM (RMM1), anti-IgD (11-26c.2a), anti-B220 (RA3-6B2), anti-CD38 (90), anti-CD138 (281-2), anti-CXCR4 (L276F12), anti-CD86 (GL1), anti-polyhistidine tag (His-tag) (AD1.1.10), and anti-Tim3 (5D12). Secondary staining for biotinylated primary Ab was done using streptavidin (BioLegend). For intracellular staining, samples were fixed with Fixation/Perm solution kit (BD Biosciences) for intracellular Ig or Foxp3 Fix/Perm buffer set (eBioscience) for staining transcription factors according to manufacturer's instruction. Samples were then intracellularly stained with anti-IgG1 (RMG1-1), anti-IgG2b (RMG2b1), anti-IgE (RME1), anti-IgA (goat anti-mouse polyclonal; SouthernBiotech), anti-Foxp3 (FJK-16S), and anti-Bcl6 (K112-91). For Fc block experiments, 10 ng/ml purified anti-mouse CD16/32 Ab (BioLegend) was used. For anti–IL-10 blocking experiments, 500 ng/ml of purified rat anti-mouse IL-10 (BD Biosciences) was used.

Sorting

Single-cell suspensions were diluted in PBS supplemented with 3% FBS with 2 mM EDTA. $CD4^+$ cells were enriched by magnetic-positive selection (Miltenyi Biotec). $CD4^+$ enriched cells were then stained and sorted as follows: TFH ($CD4^+CD19^-ICOS^+CXCR5^+Foxp3^-$) and TFR ($CD4^+CD19^-ICOS^+CXCR5^+Foxp3^+$). B cells were isolated from flow through from $CD4^+$ selection and sorted as $CD19^+CD4^-$. Single sorting was used in all of the experiments, except for gene expression profiling ones, in which double sorting was used.

Droplet-based, single-cell RNA-seq

Inguinal lymph nodes from wild-type mice immunized with NP-OVA/CFA (s.c.) for 7 d were isolated and $CD4^+$ cells by magnetic-positive selection (Miltenyi Biotec). Cells were then sorted based on $CD19^-CD4^+CXCR5^+PD1^+$ with permissive thresholds for CXCR5 and PD1 gating. Cells were then subjected to droplet-based, single-cell RNA-seq using the Chromium Single Cell Gene Expression Solution platform (10× Genomics).

Population RNA-seq

Samples were sorted as described above. RNA-seq library preparations were performed. Briefly, RNA was isolated using RNeasy Mini Kit (QIAGEN). The cDNA libraries were prepared based on modified SMARTseq2 protocol as previously described with eight amplification cycles (33, 34). The library quality was confirmed using BioAnalyzer high-sensitivity DNA chip (Agilent Technologies). RNA-seq reactions were sequenced on an Illumina HiSeq 2000 or Illumina NextSeq sequencer (Illumina) according to manufacturer's instructions, sequencing 50-bp reads.

In vitro culture assays

In vitro culture assays were performed as previously described (35). Briefly, 5×10^4 total $CD19^+CD4^-$ B cells or GC B cells ($CD19^+CD4^-Fas^+GL\text{-}7^+$) 3×10^4 TFH cells and/or 1.5×10^4 TFR cells were plated in 96-well plates along with 25 ng LPS, 5 μg anti-CD40 (BioLegend) or 2 μg/ml anti-CD3, and 5 μg/ml anti-IgM (Jackson ImmunoResearch Laboratories). Polarizing cytokines for T cell and B cell CSR are described in specific experiments. Cultures were harvested after 3–6 d as specified in specific experiments. Recombinant tetrameric mouse Fgl2-His (R&D Systems) was added into the culture as described. For analysis, B cells were gated as $CD19^+CD4^-$ cells, whereas specific isotype staining was done by intracellular staining described earlier, TFH cells were gated as $CD4^+CD19^-Foxp3^-$ cells, and TFR cells were gated as $CD4^+CD19^-Foxp3^+$ cells.

ELISA

ELISA measurements of IgG from culture supernatants and sera were performed as described previously (32, 36). For autoantibody ELISA, mouse anti-nuclear Ags (ANA; ANA/extractable nuclear Ag) Igs (total [IgA + IgG + IgM]), anti-dsDNA Igs (total [IgA + IgG + IgM]), and anti-dsDNA, IgG1-specific ELISA kits were used according to the manufacturer's instruction.

Bead-based immunoassays

Soluble mouse Ig isotype measurements were performed using mouse Ig isotyping kit (BD Biosciences), whereas soluble cytokine measurements were performed using LEGENDplex kit (BioLegend) according to manufacturers' instructions. The mouse Ig isotyping kit provides no standard curve assessment, so the results should be considered more as qualitative. The LEGENDplex kit, however, provides standard curve assessment.

Autoantigen microarray

Lupus autoantigen microarrays were constructed and developed as described (37–39). Briefly, 33 were spotted onto Epoxy slides (Arrayit, Sunnyvale, CA). The microarrays were blocked for 1 h at 37°C with 1% BSA and incubated for 2 h at 37°C with a 1:100 dilution of the test serum in blocking buffer. The arrays were then washed and incubated for 45 min at 37°C with a 1:500 dilution of a goat anti-mouse IgG detection Ab conjugated to Cy3 and anti-mouse IgM detection Ab conjugated to Cy5 (Jackson ImmunoResearch Laboratories, West Grove, PA). The arrays were scanned with a ScanArray 4000× scanner (GSI Luminomics, Billerica, MA).

ELISPOT

Ethanol-activated MultiScreenHTS IP filer plates (EMD Millipore) were coated with either 100 μl of filtered (with 0.45-μm filters) salmon sperm DNA (5 μg/ml; Thermo Fisher Scientific) or NP-OVA (10 μg/ml;

Biosearchtech) overnight at 4°C. The plates were then washed with PBS and blocked for 2 h with blocking buffer (5% FCS and 3% BSA in PBS) before they were rewashed and let dry. Fifty microliters of splenocytes in clone media (started with 5×10^5 cells per well with 1/3 serial dilutions) were plated, and 50 μl of anti-CD40 (10 μg/ml) was added per well (final concentration of 5 μg/ml). The cells were incubated at 37°C for 24 h. After that, cells and unbound cytokines were washed by incubating with PBS Tween 20 buffer for 10 min and then thoroughly rewashed. A total of 50 μl of biotin-conjugated goat anti-mouse Ig (1:350 dilution in clone media; SouthernBiotech) was then added and incubated overnight at 37°C for primary staining. After rewashing, secondary staining was done for 1 h using 50 μl of streptavidin–alkaline phosphatase (1:1000 dilution in 1% BSA in PBS; Mabtech). The plates were then washed and developed using 50 μl 5-bromo-4-chloro-3-indolyl phosphate/NBT-plus substrate (Mabtech). When spots are clearly visible under a dissecting microscope, stop the development by discarding the substrate and rinse plates with tap water thoroughly. Spots were counted manually with a dissecting microscope.

NanoString

nCounter platform (NanoString Technologies) was used according to the manufacturer's instruction. A codeset of T cells associated genes and four additional housekeeping genes were custom made.

Histology and immunohistochemistry

Spleens, lymph nodes, lungs, kidneys, livers, guts, and patches of skin were harvested and fixed in 10% formalin, paraffin embedded, and sectioned. Representative sections were stained with H&E. For immunohistochemistry, avidin–biotin immunohistochemical staining was performed on the sections with rabbit anti-mouse CD3 (Abcam, Cambridge, U.K.) and rat anti-mouse CD45R (B220; BD Biosciences) using reagents from Vector Laboratories (Burlingame, CA).

Statistical analysis for non–RNA-seq data

Statistical analysis was performed using Prism 7 (GraphPad). Differences between two groups were compared using either Kruskal–Wallis tests, followed by post hoc Dunn tests for multiple comparisons or two-tailed unpaired Welch *t*-tests (*$p < 0.05$, **$p < 0.01$, and ***$p < 0.001$). All figures show the mean ± SD.

Data analysis for single cell RNA-Seq data

The 10× sequencing outputs were processed with Cell Ranger (10× Genomics) and loaded into a Seurat object (40), which was used to scale the data, regress out unwanted axes of variation (number of unique molecular identifiers and ratio of mitochondrial unique molecular identifiers per library), and cluster the cells with the smart local moving algorithm. Default parameter values were used unless specified otherwise. Differential expression between cell clusters was performed with Seurat implementation of a Wilcoxon-based procedure, followed by Bonferroni adjustment for multiple comparisons.

Computational transcriptomic signatures

Computational signatures (Fig. 1A) were computed as described in (PMC4671824 and PMC6763499). Briefly, a signature is list of genes positively or negatively associated with a cellular state of interest with some weight (in this study, always +1 or −1). Let v be a column vector where the coordinate of a given gene is its weight or 0 if the gene is not part of the signature. Given a gene expression CPM matrix G (cells × genes), the product vector Gv gives the scores for each cell with respect to the signature.

In this study, we addressed 10× sparsity with respect to key signature transcripts by partitioning the cells into small, mutually exclusive groups (micropools of ∼5 cells each) and averaging the gene expression profiles of cells in the pool following the method outlined in (PMC6763499). We then used that average profile to compute a signature value and assigned that value as the signature score for all cells in the pool.

We defined three transcriptomic signatures. The first was an unsupervised signature based on TFR versus TFH cells (Fig. 1C, Supplemental Table I) by calling differentially expressed genes in the population RNA libraries described in the *Results* section. Libraries were aligned with Tophat2 (41), reads per transcript were counted with featureCounts (42), and differentially expressed genes were then called with DESeq2 (43) using the thresholds false discovery rate ≤ 10% and $|B| \geq 10\%$, where B is the moderated B-statistic. Signature weights were set to +1 for upregulated and −1 for downregulated genes in a TFR versus TFH comparison. The second signature (Supplemental Table I) consisted of a list of manually curated TFH-related genes (all set to have the same weight +1). The third signature (Supplemental Table I) was adapted from PMC4671824 and was based on a bulk RNA-seq comparison of natural Treg (nTreg) cells to other Th subsets (GSE14308), with +1 or −1 weights for genes upregulated or downregulated in nTreg, respectively.

Results

Fgl2 is a distinguishing marker for TFR cells

To assess potential effector molecules downstream of TFR cells, we performed a high-throughput, 10× single-cell RNA-seq assay on $CD19^-CD4^+CXCR5^+PD1^+$ T cells from draining lymph nodes of wild-type mice immunized with NP-OVA/CFA for 7 d. We used permissive thresholds for CXCR5 and PD1 gating (Supplemental Fig. 1A) to include cells like non-TFR Treg cells, which would be useful for comparative analyses. The permissive gating also allows us to gain a complete statistical representation of TFR cells states (44). More restrictive gating would preferentially exclude TFR states in which CXCR5 or PD1 are present but are expressed at low levels. The inclusion of such transitional state is crucial for identifying novel regulators that drive development of different cell states. The use of droplet-based single cell RNA-Seq, which typically sequences thousands of cells in a single run, assured that TFR cells would stochastically be represented in the data despite the permissive CXCR5 and PD1 gating thresholds. We applied a standard 10× quality control and data-processing pipeline (*Materials and Methods*) to quantify the transcriptome of 12,628 cells, which we subsequently clustered with the unsupervised smart local moving algorithm (45).

For each of the cells, we computed quantitative signatures of T cell identity (34) and visualized them with *t*-distributed stochastic neighbor embedding (*t*-SNE) plots. We identified four pertinent clusters of interest, one corresponding to TFR cells with enrichment in both Treg and TFH signatures (Fig. 1A; Se_2_Treg/TFR in green), one corresponding to non-TFR Treg cells with no TFH signature enrichment (Fig. 1A; Se_4_Treg in purple), and two corresponding to TFH cells (Fig. 1A; Se_3_TFH and Se_7_TFH in orange and pink). We confirmed the identity of these clusters using three computational transcriptomic signatures (Fig. 1A; *Materials and Methods*; Supplemental Table I). The first signature was derived from differential expression in population RNA-seq of sorted TFR and TFH cells ($CD19^-CD4^+CXCR5^+PD1^+Foxp3^+$ and $CD19^-CD4^+CXCR5^+PD1^+Foxp3^-$, respectively) from draining lymph nodes of Foxp3-IRES-eGFP reporter mice immunized with NP-OVA (Supplemental Fig. 1B, 1C). The second signature was a hand-curated list of TFH-associated genes, and the third signature was a computational signature distinguishing nTreg cells from other Th subsets. Next, we verified the identification of these clusters through genes differentially enriched in them. As expected, Se_2_Treg/TFR and Se_4_Treg clusters express Foxp3, whereas TFH-associated genes, including *Cxcr5*, programmed cell death 1 (*Pdcd1*), *Icos*, *Maf*, and, to a lesser extent, *Bcl6*, are only enriched in the Se_2_Treg/TFR cluster. It is likely that the Se_2_Treg/TFR cluster not only includes TFR cells but also non-TFR effector Treg cells with enriched expression of *Prdm1* (encoding BLIMP1) and *Tnfrsf18* (encoding GITR). The two TFH clusters, in contrast, are enriched in the TFH marker genes with minimal Foxp3 enrichment (Fig. 1B, Supplemental Fig. 1E). We hypothesized that the transcriptomic program of TFR cells should reflect a combination of TFH and Treg elements. Indeed, the differential expression between Se2 (Treg/TFR) and Se4 (Treg) was well aligned with the differential expression between TFH and non-TFH cells (Se3 and Se7 versus the other cluster shown in Fig. 1A) (Supplemental Fig. 1F). Two notable exceptions were *Cxcr5*

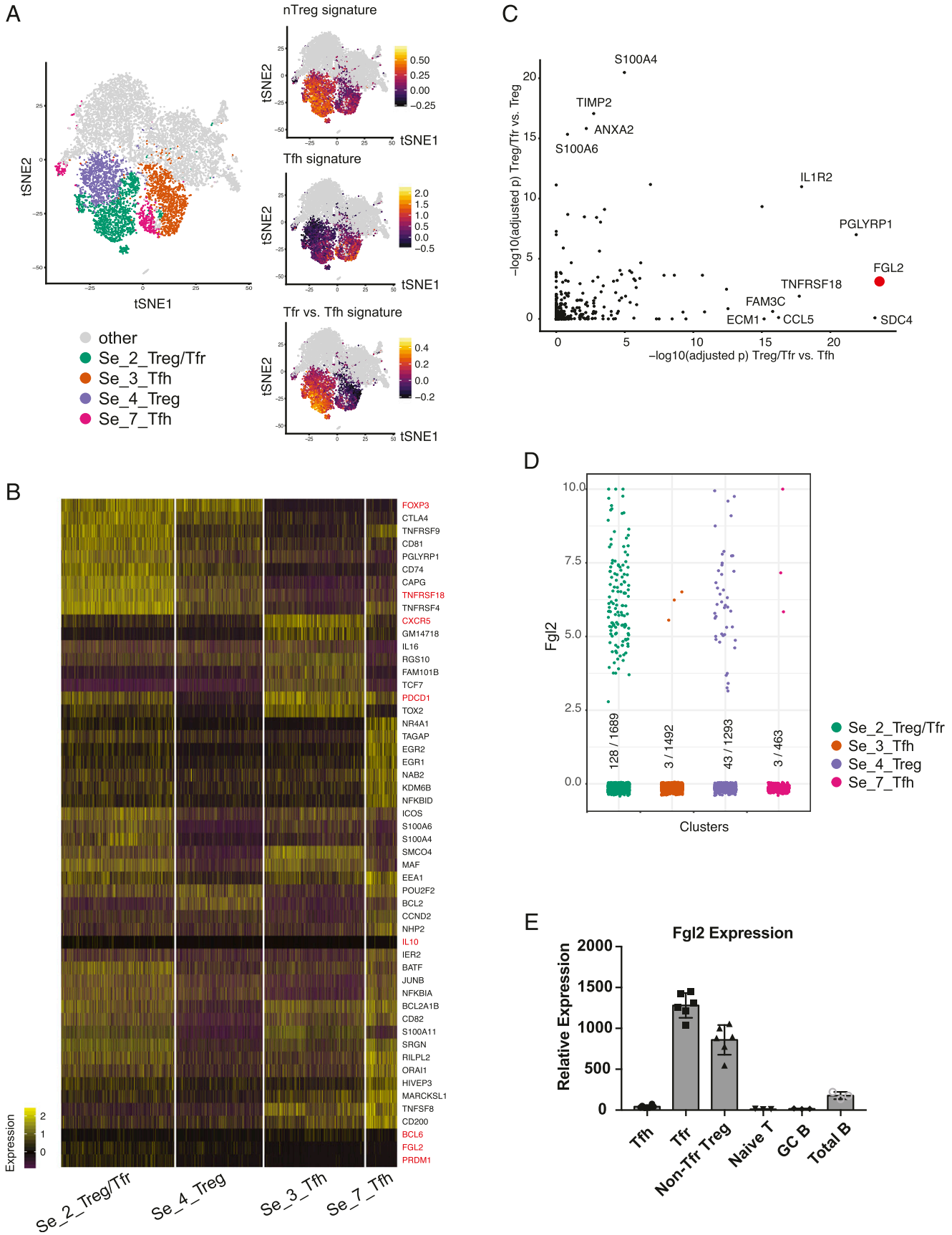

FIGURE 1. Fgl2 is a distinguishing marker of TFR cells. (**A**) *t*-SNE visualization of 10× single-cell transcriptomes. Four relevant clusters of interest (left) are shown, whereas the gray dots correspond to cells belonging to other clusters. The other three panels present values of computational signatures, allowing one to assign identities to the clusters (*Materials and Methods*). (**B**) Genes that are differentially expressed between the clusters are shown. All of the genes, except for the ones in red, are the top differentially expressed genes in the corresponding clusters. The genes in red, on the other hand, are assigned manually as they are known TFH/Treg marker genes, as well as Fgl2. (**C**) Markers of TFR cells should be *(Figure legend continues)*

and *Crip1*. *Cxcr5* distinguished TFH from non-TFH but not Se2 from Se4. *Crip1* was significantly downregulated in TFH compared with non-TFH but upregulated in Se2 compared with Se4. Interestingly, *Hif1a*, which is associated with an effector over a tolerant Th phenotype (46, 47), was significantly upregulated in Se2 (Treg and TFR) over Se4 (Treg).

To screen for potential novel TFR effector molecules, we sought genes that are 1) preferentially detected in the Se_2_Treg/TFR cluster compared with the two TFH clusters, 2) preferentially detected in the Se_2_Treg/TFR cluster compared with the Se_4_Treg cluster, and 3) associated with an extracellular secreted product (Gene Ontology: 0005576). Through these criteria, we identified *Fgl2* among the top genes (Fig. 1C, 1D). Additionally, we investigated the population RNA-seq data on TFR cells and TFH cells (Supplemental Fig. 1C) and confirmed that *Fgl2* was among the top genes encoding secreted proteins differentially expressed by TFR cells when compared with TFH cells (Supplemental Fig. 1D). Quantitative PCR (qPCR) results confirmed that TFR cells expressed a high level of *Fgl2* in comparison with TFH cells, whereas non-TFR Treg cells also expressed high levels of *Fgl2* as described previously (48). In contrast, naive T cells, total $CD19^+CD4^-$ B cells, and GC B cells expressed low levels of *Fgl2* if any (Fig. 1E).

Fgl2 directly binds B cells and TFH cells

To test the hypothesis that Fgl2 is an effector molecule of TFR cells, we first investigated whether Fgl2 directly binds to B cells and TFH cells, as Fgl2 was previously demonstrated to bind to dendritic cells, peritoneal macrophages, and total splenic B cells (49, 50). Using recombinant Fgl2 protein with a His-tag, we showed that Fgl2 also binds in a dose-dependent fashion to total $CD19^+$ B cells in draining lymph nodes of NP-OVA/CFA–immunized mice for 7 d (Fig. 2A, 2B), whereas His-tag alone does not (Supplemental Fig. 2A). Further analysis of B cell subsets revealed preferential binding of Fgl2 to LZ GC B cells, defined as $CD19^+CD38^-Fas^+GL\text{-}7^+CXCR4^-CD86^+$ cells (51) (Fig. 2C, 2D, Supplemental Fig. 2B, 2C). The preferential binding to GC B cells, particularly LZ GC B cells, implies its relevance to TFR functions as suppressors of GCs. Fgl2 also preferentially binds to TFH cells, defined as $CD19^-CD4^+Foxp3^-CXCR5^+PD1^+$ cells, in a dose-dependent fashion (Fig. 2E, 2F).

Fgl2 has been reported to bind two receptors: Fcgr2b and Fcgr3 (49). Because Fgl2 can bind to both B cells and TFH cells, we studied if the binding was dependent on the two receptors and how the receptors are expressed. Treatment with Fc block, which antagonized both receptors, partially suppressed Fgl2 binding both on LZ GC B cells, and TFH cells (Fig. 2G, Supplemental Fig. 2B–D). Moreover, we found that, at RNA level, Fcgr2b is highly expressed on GC B cells and, at a lower level, on TFH cells, whereas Fcgr3 is expressed on TFR cells and, to a lower extent, on GC B cells (Fig. 2H). We were unable to properly detect the two receptors at protein level, as available Abs for flow cytometry were not able to discriminate Fcgr2b and Fcgr3.

Fgl2 directly regulates B cells

Next, we analyzed the effects of Fgl2 on B cells and TFH cells. We cultured sorted total splenic $CD19^+CD4^-$ B cells from nonimmunized mice in different conditions in the presence of Fgl2 and found that Fgl2 limits B cells survival and proliferation under anti-IgM condition but not in LPS and anti-CD40 conditions (Supplemental Fig. 3A–C).

To investigate if Fgl2 influences B cell CSR, we cultured sorted total $CD19^+CD4^-$ splenic B cells from nonimmunized mice in cytokine-polarizing conditions in the presence of LPS with or without recombinant Fgl2 for 4 d. The presence of recombinant Fgl2 inhibited IgG1 and IgE CSR under IL-4–polarizing conditions, but modestly enhanced IgG2b under IFN-γ–polarizing conditions as assayed by intracellular staining and cytometric bead array. Similar results were also observed when total $CD19^+CD4^-$ splenic B cells from mice immunized with NP-OVA/CFA for 7 d were used (Fig. 3A–C, Supplemental Fig. 4A, 4B) as well as when sorted GC B cells ($CD19^+CD4^-Fas^+GL\text{-}7^+$) from mice immunized with NP-OVA/CFA for 14 d were cultured in the presence of anti-CD40 Abs (Supplemental Fig. 4C). These findings suggested that B cell CSR regulation by Fgl2 is context dependent and isotype selective. The impact of Fgl2 on B cell CSR was not dependent solely on either Fcgr2b or Fcgr3, as Fgl2 still retained its effects on single-knockout B cells. However, although we could not generate double-knockout mice because of the close proximity of loci encoding the two receptors, the presence of Fc block abrogated the effects of Fgl2 on B cell CSR but never reached the wild-type level, suggesting that there may be additional receptors through which Fgl2 must act or that the Fc block does not completely block the receptors (Fig. 3A–C, Supplemental Fig. 4C).

Fgl2 directly regulates TFH cells

To test the effects of Fgl2 on TFH cells, we sorted TFH cells and cultured them with plate-bound anti-CD3 and anti-CD28. The addition of Fgl2 suppressed production of most secreted cytokines tested, including IFN-γ, IL-2, IL-4, IL-10, IL-17A, IL-21, and IL-13 in vitro (Supplemental Fig. 5A). However, these data should be interpreted with caution as expression of TFH-associated genes, including *Bcl6*, *Maf*, *Cxcr5*, and *Icos*, was lost upon in vitro activation by anti-CD3/anti-CD28 in the absence of B cells (Supplemental Fig. 5B). The addition of total $CD19^+CD4^-$ B cells from the same immunized mice we harvested, TFH cells in the TFH/B cell coculture in the presence of soluble anti-CD3, and IgM (32, 35) resulted in only secreted IL-13 and IL-5, but not IFN-γ, being suppressed in the presence of soluble Fgl2 (Fig. 4A). Interestingly, upon Fgl2 treatment, *Il4* mRNA was decreased, whereas *Il21* was significantly upregulated in TFH cells (Fig. 4B). B cell survival in the presence of TFH cells was not affected (Supplemental Fig. 3D) unless B cells and TFH cells were from immunization with different Ags (Supplemental Fig. 3E). This selective suppression of type 2 cytokines was associated with a selective decrease in IgG1 production (Fig. 4A). However, whether the decrease in IgG1 production was due to the altered cytokine profile of the TFH cells is unclear, as Fgl2 was demonstrated earlier to directly suppress IgG1 CSR on B cells (Fig. 3A).

Fgl2 regulates Ab responses through TFH cells in vitro

To investigate whether the role of Fgl2 in regulating Ab responses is dependent on TFH cells, we used a well-characterized coculture system previously described (35). As TFH cells only express

enriched in Treg/TFR cluster compared with both TFH and non-TFR Treg clusters. Each dot corresponds to a gene associated with an extracellular secreted product (Gene Ontology: 0005576). Its *x*- and *y*-values are Benjamini-Hochberg–adjusted *p* values for hypergeometrically testing whether detections of the gene are enriched in the given comparisons. (**D**) Fgl2 expression in the four clusters. (**E**) High expression of Fgl2 by TFR cells was confirmed by TaqMan qPCR. The single-cell RNA-seq experiment was performed once with samples run on three different lanes. The qPCR results are representative of three independent experiments with the plot showing the mean ± SD.

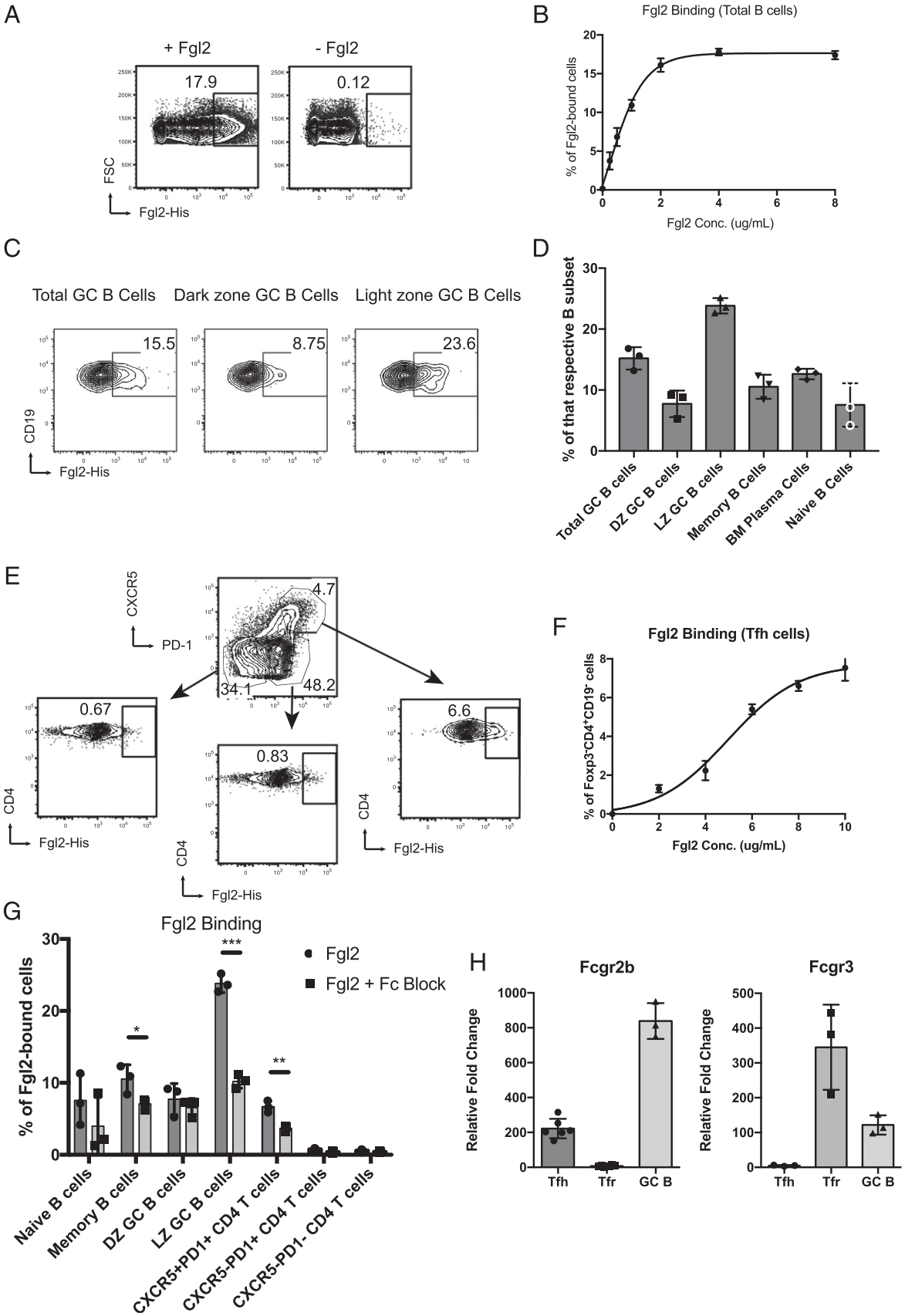

FIGURE 2. Fgl2 directly binds and regulates B cells and TFH cells in vitro. (**A**–**D**) Draining lymph node cells or bone marrow cells from NP-OVA/CFA–immunized mice for 14 d were stained and treated with recombinant Fgl2 with His-tag, followed by secondary anti-His Abs with fluorophore (allophycocyanin or phycoerythrin). (A and B) Fgl2 binds to total B cells ($CD19^+CD4^-$) from NP-OVA/CFA–immunized mice for 7 d, with the titration curve showing a dose-dependent binding. (C and D) Fgl2 binds to different B cell subsets gated as followed: total GC B cells ($CD19^+CD38^-Fas^+GL\text{-}7^+$), dark-zone (DZ) GC B cells ($CD19^+CD38\text{-}Fas^+GL\text{-}7^+CXCR4^+CD86^-$), and LZ GC B cells ($CD19^+CD38^-Fas^+GL\text{-}7^+CXCR4^-CD86^+$). Gating for the other B cell subsets and representative FACS plot can be found in Supplemental Fig. 2A–C (**E** and **F**) Fgl2 preferentially binds to *(Figure legend continues)*

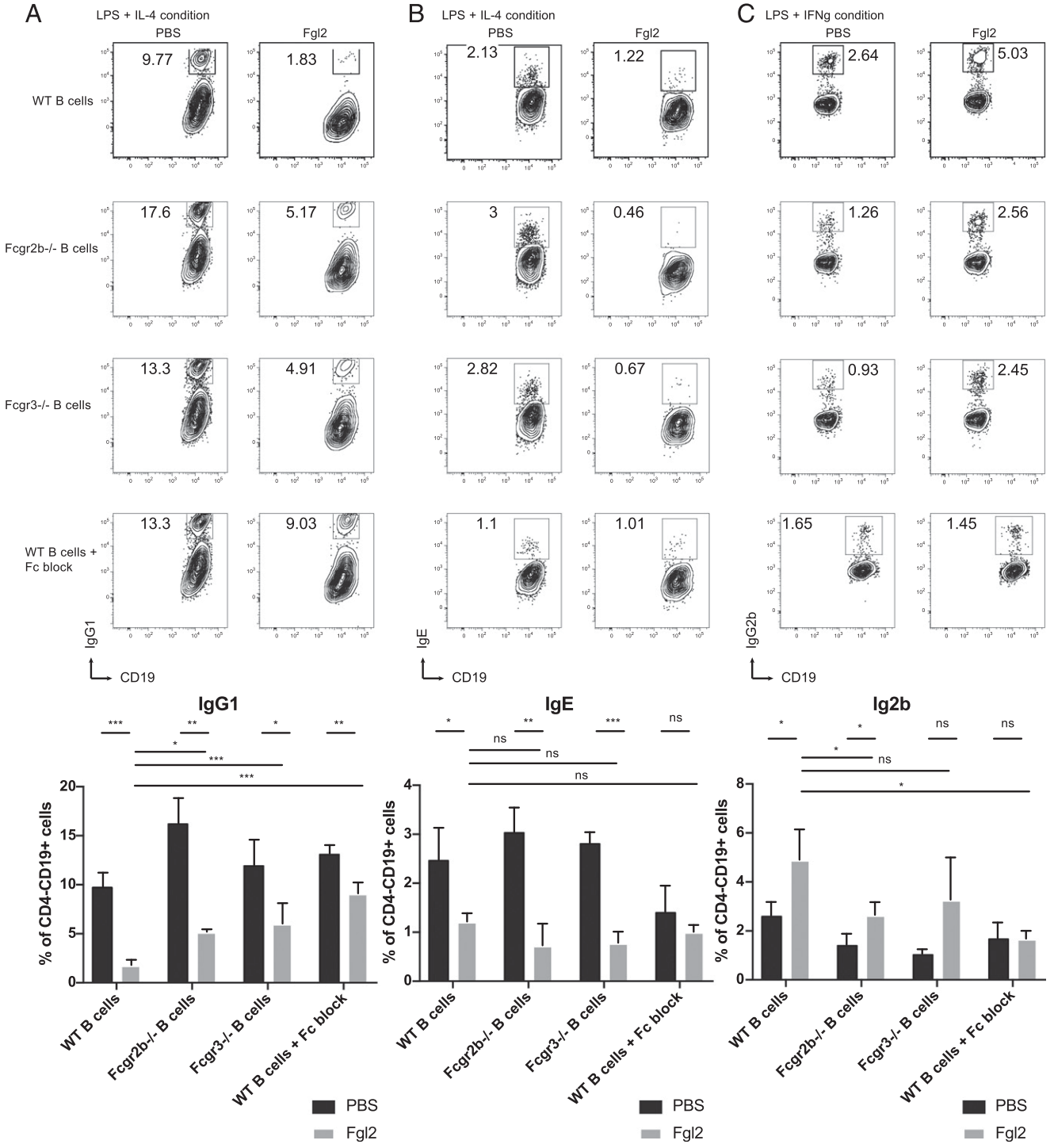

FIGURE 3. Fgl2 regulates B cell CSR in vitro (**A**–**C**) Effect of Fgl2 on B cell CSR: in vitro class switching assay. Sorted total B cells ($CD19^+CD4^-$), nonimmunized wild-type, $Fcgr2b^{-/-}$, or $Fcgr3^{-/-}$ mice for 7 d were cultured in LPS + IL-4 (IgG1 and IgE) or LPS + IFN-γ (IgG2b) for 4 d in the presence or absence of Fc block. Switched isotypes were detected by flow cytometry. All plots show the mean ± SD with $n = 3$ in each group. $*p < 0.05$, $**p < 0.01$, $***p < 0.001$, between two groups, using Kruskal–Wallis tests, followed by post hoc Dunn tests for multiple comparisons. n.s, not significant.

Fcgr2b, but not Fcgr3, we tested whether the Fgl2 would regulate IgG1 suppression through TFH cells deficient in Fcgr2b. Addition of Fgl2 to wild-type B cells and TFH cultures resulted in significant inhibition of IgG1 production. Although coculturing wild-type B cells with $Fcgr2b^{-/-}$ TFH cells showed no significant difference in IgG1 level in the absence of Fgl2, the suppression by

TFH cells ($CD19^+CD4^-Foxp3^-CXCR5^+PD1^+$) with the titration curve showing a dose-dependent binding. (**G**) Fgl2 binding was partially abolished in both LZ GC B cells and TFH cells in the presence of Fc block. (**H**) Expression of Fcgr2b and Fcgr3 were assessed by TaqMan qPCR in sorted TFH cells, TFR cells, and GC B cells from mice immunized with NP-OVA/CFA 7 d earlier. The summary results were pooled from two to three independent experiments. All plots show the mean ± SD. $*p < 0.05$, $**p < 0.01$, $***p < 0.001$, between two groups, using two-tailed unpaired Welch *t*-tests. n.s, not significant.

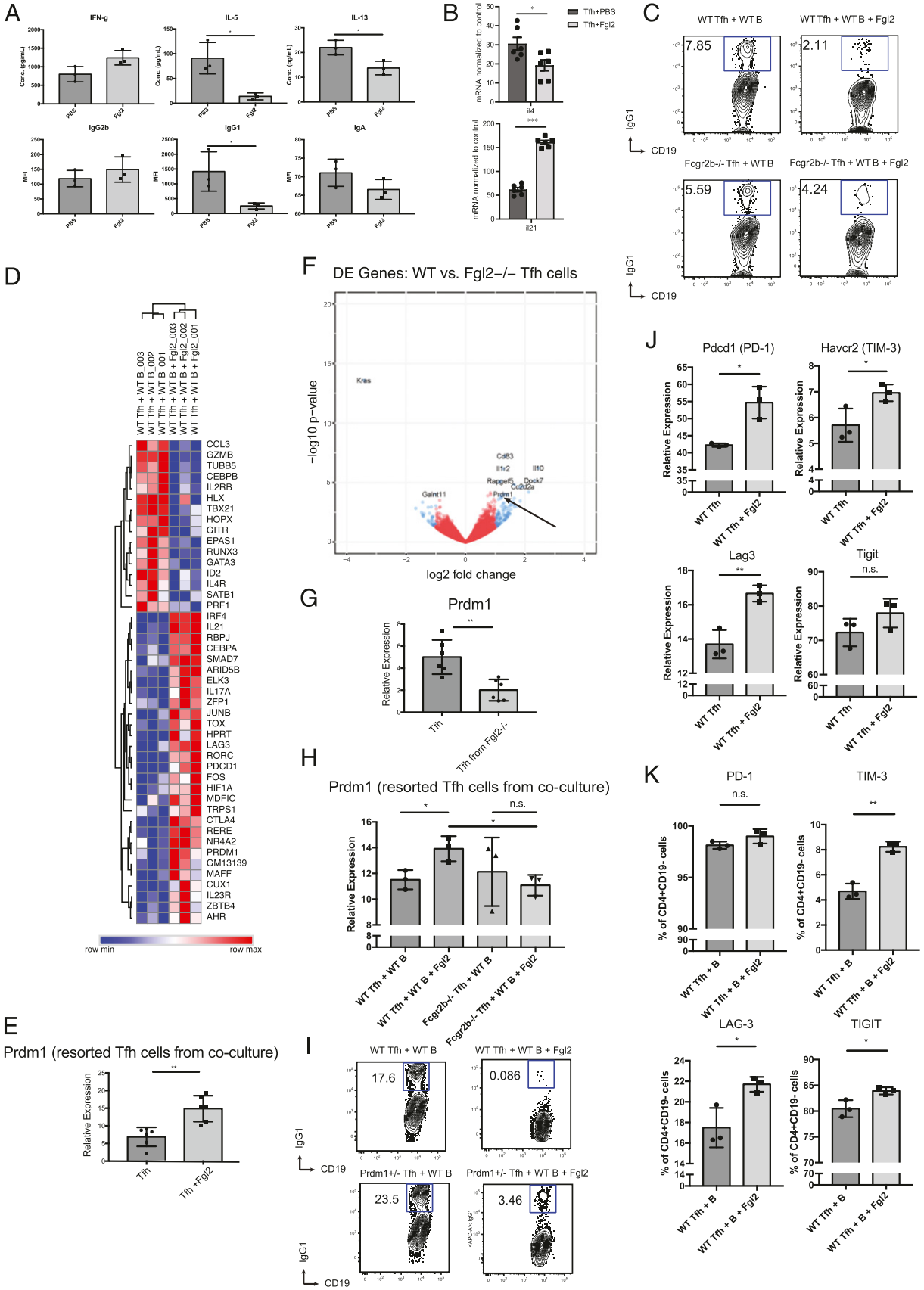

FIGURE 4. Effect of Fgl2 on B cells in the context of TFH presence. (**A**) Effects of Fgl2 on TFH/B cell coculture: sorted TFH cells were cocultured with sorted total B cells from the same immunized mice in the presence of soluble anti-CD3 and anti-IgM with or without Fgl2 for 3 d. Cytokines were detected by bead-based LEGENDplex kit and Ab isotypes were detected by bead-based mouse Ig isotyping kit. (**B**) Sorted TFH cells were cocultured with sorted total B cells from immunized mice in the presence of soluble anti-CD3 and anti-IgM with or without Fgl2 for 3 d. T cells were then resorted and subjected to NanoString gene expression profiling. Bar chart exhibiting Il4 and Il21 mRNA normalized expression. (**C**) Wild-type TFH cells or Fcgr2b$^{-/-}$ TFH cells were cocultured with wild-type B cells from immunized mice in cells in the presence of soluble anti-CD3 and anti-IgM with or *(Figure legend continues)*

exogenous Fgl2 was partially rescued when Fcgr2b$^{-/-}$ TFH cells were present in the culture (Fig. 4C, Supplemental Fig. 6A, 6B), suggesting that the Fcgr2b receptor expression on TFH cells can regulate IgG1 CSR in the presence of exogenous Fgl2.

To further investigate potential downstream molecules of TFH cells that modulate IgG1 CSR in response to Fgl2, we resorted TFH cells after the coculture with B cells and Fgl2 and analyzed gene expression profiling using the NanoString platform. We failed to see inhibition of TFH-related genes, including *Bcl6*, *Pdcd1*, and *Il21*; these genes were in fact upregulated. There was induction of genes associated with TFH functional suppression, including *Ctla4* and *Prdm1* (Fig. 4D, 4E). The effect of Fgl2 on *Prdm1* expression in TFH cells was also observed in vivo, as *Prdm1* was among the top genes differentially expressed genes when expression analysis was undertaken between wild-type and Fgl2$^{-/-}$-derived TFH cells, and the reduced Prdm1 expression in TFH cells from Fgl2$^{-/-}$ mice was confirmed by qPCR (Fig. 4F, 4G, Supplemental Fig. 5C, 5D). *Prdm1* induction by Fgl2 in TFH cells was dependent on Fcgr2b on the cells, as Fcgr2b-deficient TFH cells failed to upregulate *Prdm1* in response to Fgl2 treatment as measured by qPCR from T cells resorted from TFH/B cell coculture experiments (Fig. 4H).

To test if *Prdm1* is downstream of Fgl2 in TFH cells, we cocultured wild-type B cells with *Prdm1*-deficient TFH cells. Notably, TFH cells deficient in both *Prdm1* copies (*Prdm1*$^{-/-}$) failed to induce IgG1 in B cells (Supplemental Fig. 6C–E) even though the gene was shown to be antagonistic of Bcl6 (7). Thus, we hypothesized that such functions might require some level of *Prdm1* expression, and the regulation is rather dependent on some *Prdm1* level, but not in the context of its total absence. In fact, mice deficient only in one copy of *Prdm1* were previously shown to possess phenotype distinct from those deficient in both (52). Using TFH cells from mice deficient in one copy of *Prdm1* (*Prdm1*$^{+/-}$), we found that those TFH cells were as capable of inducing IgG1 in B cells as wild-type control TFH cells, whereas they conferred modest but significant resistance to Fgl2-mediated suppression of IgG1 B cells upon Fgl2 treatment (Fig. 4I, Supplemental Fig. 6F, 6G), suggesting that the effects of Fgl2 on TFH cells have some dependency on *Prdm1*. Notably, the rescues of inhibition mediated by Fgl2 in *Prdm1*$^{+/-}$ TFH cells is modest, suggesting that other molecules are likely to be involved in addition to Prdm1. In fact, we have previously shown that multiple transcription factors cooperate to mediating a defined phenotype/function, and we predict that modest effects observed by loss of *Prdm1* in abrogating Fgl2-derived inhibition may be due to 1) use of *Prdm1* heterozygous mice; 2) other transcription factors might be playing a compensatory or additive role in mediating inhibitory function of Fgl2 (53); and 3) Fgl2 may use other mechanisms in addition to induction of *Prdm1* in mediating its inhibitory function.

As *Prdm1* was previously shown to be involved in regulating expression of IL-10 and coinhibitory gene module (53), we also checked if Fgl2 had effects on checkpoint molecules on TFH cells. We found that Fgl2 induced upregulation of multiple coinhibitory, checkpoint molecules, including PD1, TIM3, LAG3, and TIGIT on TFH cell cocultured with B cells measured at both mRNA and protein levels (Fig. 4J, 4K, Supplemental Fig. 6H). Furthermore, whereas we found a decreased expression of *Il10* in Fgl2$^{-/-}$ TFH cells (Supplemental Fig. 6I), addition of Fgl2 to the cultures had no effect on IL-10 expression (Supplemental Fig. 6J). To study the role of IL-10 on B cells, we cocultured TFH and B cells in presence or not of Fgl2 and found that IL-10 blockade did not prevent humoral response inhibition upon Fgl2 treatment (Supplemental Fig. 6K). This indicates an IL-10–independent role of Fgl2 on B cell responses in vitro. Because we have previously observed that *Prdm1* is critical for the induction of module of checkpoint molecules, expression of the module further supports that Prdm1 and molecules downstream of *Prdm1* are also induced by Fgl2. Taken together, the results suggest that Fgl2 can partially suppress IgG1 in B cells through modulation of *Prdm1* level in TFH cells, potentially antagonizing *Bcl6* (7) in an Fcgr2b-dependent fashion, whereas the molecule also induces expression coinhibitory molecules on TFH cells.

Fgl2 regulates Ab responses in vivo

To determine if Fgl2 modulates Ab responses in vivo, we analyzed Ab production in Fgl2-deficient mice. Although young, 8 wk old, Fgl2$^{-/-}$ showed no significant differences in total serum Ab isotypes (Supplemental Fig. 7A), 20-wk-old Fgl2$^{-/-}$ mice had significantly elevated total serum IgG1, IgG2a, IgA, and IgE spontaneously (Fig. 5A). We also analyzed Peyer's patches (PP) where TFH cells and GCs are present at steady-state, and we found that Fgl2$^{-/-}$ mice had increased PP IgA^{+} B cells, GC B cells, TFH cells, and TFR cells but a decreased total number of Treg cells (which include TFR cells) (Fig. 5B, 5C). Elevated free fecal IgA was also observed even though the frequency of IgA-coated bacteria was reduced (Fig. 5B, Supplemental Fig. 7B). These findings suggested that Ab responses at steady-state were dysregulated with age in the absence of Fgl2 in vivo.

Next, we wanted to see if Fgl2 could affect Ag-specific responses. We immunized wild-type and Fgl2$^{-/-}$ mice with NP-OVA emulsified in CFA. At day 21, we detected significantly enhanced NP-specific IgG1, but not NP-specific IgG2b, by ELISA in Fgl2$^{-/-}$ mice (Fig. 5D). Interestingly, examination at an earlier time point (day 10) when GC B cells and TFH cells were still present showed no significant difference in the frequency of total GC B cells and, surprisingly, significant decrease in the frequency of NP-specific GC B cells (Supplemental Fig. 7C).

without Fgl2 for 3 d. IgG1 in B cells was detected by flow cytometry. (**D**) Heatmap showing the filtered genes based on differential expression over two folds, whereas $p < 0.05$ using NanoString gene expression profiling. (**E**) *Prdm1* expression was evaluated by TaqMan qPCR. (**F**) TFH cells were sorted from wild-type or Fgl2$^{-/-}$ mice and were subjected to RNA-seq. Some of the top differentially expressed genes were shown in the volcano plot. *Prdm1* was among the top genes differentially expressed, and its expression was confirmed by TaqMan qPCR (**G**). (**H**) Same experiment settings as in (C). However, T cells were then resorted and subjected to TaqMan qPCR to measure *Prdm1* expression. (**I**) Control TFH cells (Prdm1$^{fl/fl}$ or Prdm1$^{fl/+}$ with CD4cre^{-}) or Prdm1$^{+/-}$ (Prdm1$^{fl/+}$ with CD4cre^{+}) TFH cells were cocultured with wild-type B cells from immunized mice in cells in the presence of soluble anti-CD3 and anti-IgM with or without Fgl2 for 3 d. IgG1 in B cells was detected by flow cytometry. (**J**) Same experiment settings as in (A). Resorted T cells were subjected to TaqMan qPCR to measure *Prdm1*, *Havcr2*, *Lag3*, and *Tigit* expression. (**K**) Same experiment settings as in (A). Protein expression of PD1, TIM3, LAG3, and TIGIT were detected by flow cytometry. The summary results were pooled from two to four independent experiments, except for the NanoString gene expression and RNA-seq profiling, which were performed once with $n = 3$ in each experiment group. All plots show the mean ± SD. *$p < 0.05$; **$p < 0.01$, ***$p < 0.001$, between two groups in all but gene expression profiling data, using two-tailed unpaired Welch *t*-tests except for (G), in which Kruskal–Wallis test, followed by post hoc Dunn test for multiple comparisons was used. n.s, not significant.

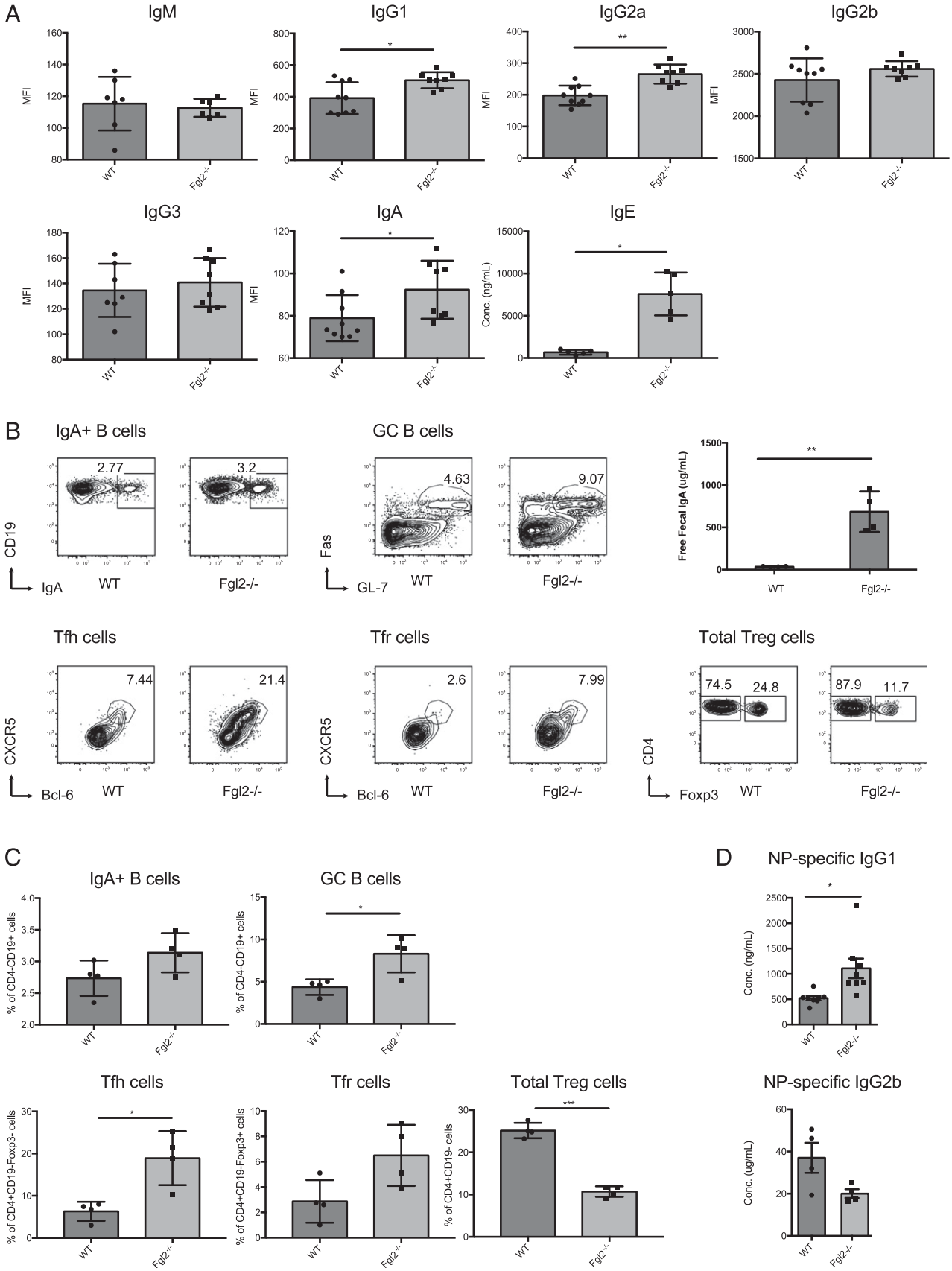

FIGURE 5. Fgl2 regulates Ab responses in vivo. (**A**) Serum Ab isotypes in 20-wk-old wild-type and Fgl2$^{-/-}$ mice were detected by bead-based mouse Ig isotyping kit and ELISA (for IgE). The mouse Ig isotyping kit provides no standard curve assessment, so the results should be considered more as qualitative. (**B** and **C**) PP of 20-mo-old wild-type and Fgl2$^{-/-}$ mice were immunophenotyped by flow cytometry for IgA^{+} B cells, GC B cells, TFH cells, TFR cells, and total Treg cells. Free fecal IgA was measured by ELISA. (**D**) Wild-type and Fgl2$^{-/-}$ mice were immunized with NP-OVA (s.c.) in CFA for 21 d, and NP-specific isotypes were detected by ELISA. The results were pooled from three independent experiments. All plots show the mean ± SD. *$p <$ 0.05, **$p < 0.01$, ***$p < 0.001$, between two groups, using two-tailed unpaired Welch t-tests. n.s, not significant.

Fgl2 from TFR cells regulates Ab responses in vitro and in vivo

Because Fgl2 affected the numbers of both TFH cells and TFR cells in vivo (Supplemental Fig. 7D, 7E) and Fgl2 may come from other cellular sources, including conventional Treg cells, we used coculture and transfer experiments to study the contribution of Fgl2 from TFR cells in the contexts in which the number of TFH cells and TFR cells are equivalent. To address whether Fgl2 from TFR cells modulates Ab responses in vitro, sorted total $CD19^+$ B cells from the immunized mice were cocultured with TFH cells and wild-type or $Fgl2^{-/-}$ TFR cells in the presence of soluble anti-CD3 and anti-IgM Abs for 3 d. We used $Fgl2^{-/-}$ B cells in this system to make sure that the main source of Fgl2 will come from TFR cells, as B cells could produce some level of Fgl2 (Fig. 1E). As expected, the addition of wild-type TFR cells suppressed IgG1 CSR, as shown by intracellular IgG1 staining and Ig bead array on secreted IgG1, whereas using $Fgl2^{-/-}$ TFR cells partially rescued it. The addition of exogenous Fgl2 also further suppressed IgG1 CSR in all conditions (Fig. 6A–C). Non-TFR Treg cells, which express Fgl2 (Fig. 1E), did not significantly suppress IgG1 CSR, and Fgl2 depletion in non-TFR Treg cells resulted in no significant difference in the suppression (Fig. 6D–F), suggesting the presence of TFR-specific effects that render Fgl2 functional at physiological concentration. Such findings demonstrated that Fgl2 from TFR cells suppress IgG1 responses in vitro.

Next, we sought to investigate if Fgl2 from TFR cells regulates Ab responses in vivo. The experimental scheme is shown in Fig. 6G. In short, we sorted TFH cells and TFR cells from mice immunized 7 d earlier with NP-OVA/CFA. Wild-type TFH cells were cotransferred with either wild-type TFR cells or $Fgl2^{-/-}$ TFR cells into $CD28^{-/-}$-recipient mice, which lacked endogenous TFH/TFR cells as previously described (19, 32). The recipient mice, along with TFH-only transfer and no-transfer controls, were then immunized with NP-OVA/CFA. At day 21, serum NP-specific IgG1 levels were significantly enhanced in mice receiving $Fgl2^{-/-}$ TFR cells (Fig. 6H). GC B cells, TFH cells, and TFR cells were analyzed on day 7 after recall immunization. The frequency of NP-specific GC B cells in mice receiving $Fgl2^{-/-}$ TFR cells was slightly but significantly elevated, whereas the frequency of TFH cells and TFR cells were not significantly different (Fig. 6I). Collectively, the data suggested that Fgl2 from TFR cells regulates IgG1 and GC responses in vivo without affecting gross TFH/TFR cell frequencies.

Fgl2 is required for autoantibody controls

We then asked whether NP-OVA/CFA immunization alone would be sufficient to induce autoreactive B cells in young $Fgl2^{-/-}$ mice, as influenza infection was previously shown to induce anti-dsDNA Abs in mice specifically deficient in TFR cells (22). ELISPOT results showed that $Fgl2^{-/-}$ mice and $CD28^{-/-}$ control mice, which completely lacked both TFH and TFR cells, had a significant increase in inguinal lymph node anti-dsDNA (total Ig) Ab-secreting cells (ASCs) with the peak at day 21 before the level started to go down (Fig. 7A), whereas only wild-type and $Fgl2^{-/-}$ mice, but not $CD28^{-/-}$ control mice, have elevated inguinal lymph node anti–NP-OVA (total IgG) ASCs starting from day 7 (Fig. 7B). Moreover, no significant differences in systemic levels of autoantibodies were observed, as shown by the level of serum anti-dsDNA and ANA. The data suggested that although $Fgl2^{-/-}$ mice still have functional total IgG ASCs against a foreign Ag despite some alterations in IgG isotypes demonstrated earlier, they failed to control local and transient expansion of autoreactive B cells during inflammation. This enhancement of autoreactive B cell responses strongly supports Fgl2 as a TFR effector molecule that controls autoimmunity.

To test if Fgl2 from TFR cells was relevant to the phenotype we saw in $Fgl2^{-/-}$ mice, we asked if transfer of TFR cells into $CD28^{-/-}$ mice, which lacked TFR cells and failed to control expansion of anti-dsDNA ASCs, would reverse the phenotype and whether the reversion was Fgl2 dependent. In fact, transfer of 10,000 wild-type TFR cells into $CD28^{-/-}$ mice significantly suppressed expansion of anti-dsDNA ASCs upon NP-OVA/CFA immunization, as measured by ELISPOT on day 21. However, the transfer of $Fgl2^{-/-}$ TFR cells in the same scheme resulted in significantly inferior suppression of such expansion (Fig. 7C), suggesting that Fgl2 from TFR cells can at least partially suppress autoreactive B cells in vivo.

Aged $Fgl2^{-/-}$ mice (7–12 mo) deficient in Fgl2 have previously been shown to have impaired Treg function and develop glomerulonephritis (31). However, autoantibody levels have not been investigated. To assess whether there were active autoreactive B cells in aged 12-mo-old $Fgl2^{-/-}$ mice with no external perturbation, we performed ELISPOT experiments to detect anti-dsDNA ASCs using total splenocytes from aged $Fgl2^{-/-}$ mice and age-matched wild-type controls and found that aged $Fgl2^{-/-}$ mice had elevated splenic anti-dsDNA (total Ig) ASCs (Fig. 7D). To determine if the elevation of autoantibodies was systemic, we measured serum Abs and found elevated levels of anti-dsDNA IgG1 and ANA in aged $Fgl2^{-/-}$ mice as compared with age-matched wild-type controls (Fig. 7E, 7F). A more comprehensive detection was performed using lupus-associated autoantigen microarrays. We observed elevation of multiple autoantibodies against lupus-associated autoantigens, including ssDNA, α elastin, β2 glycoprotein, dsDNA, U1 small nuclear ribonucleoprotein, and collagen x, in aged $Fgl2^{-/-}$ mice, and the distribution of IgM/IgG isotypes also reflected disease severity based on histological data (Fig. 7G, 7H). Although this increase in autoantibodies was not seen with all autoantigens, and in fact, for some Ags like histone 2b, the autoantibody level was decreased. This suggests that the loss of Fgl2 does not uniformly increase in the production of Abs to all autoantigens.

Aged $Fgl2^{-/-}$ mice developed inflammatory, lupus-like autoimmunity

Forty-two percent of the aged, 12-mo-old, $Fgl2^{-/-}$ mice in our cohort spontaneously developed a skin-associated phenotype that included patches of hair loss, hyperkeratosis, and dermatitis (Fig. 8A, 8B). Histological analysis of the skin showed signs of surface ulceration, hyperkeratosis, elongation of rete ridges, dermal scarring, epidermolysis, follicular plugging (Fig. 8C, arrow), and basal cell discohesion (Fig. 8C, arrow). Infiltration of T and B cells into the skin was also observed (Fig. 8C). A total of 18% of the aged mice also had spontaneous GC cell phenotype in spleens (Fig. 8A, 8D). The results suggested that the loss of Fgl2 led not only to systemic elevation of lupus-associated autoantigens but also clinical manifestations of inflammatory diseases.

Discussion

We have used single-cell transcriptome analysis and population RNA-seq to identify Fgl2 as a top-ranking gene in TFR cells. Moreover, we showed that Fgl2 is preferentially expressed in TFR cells as compared with TFH cells, naive T cells, and GC B cells, and it is critical in controlling type 2 Ab responses and autoreactive B cell responses spontaneously arising during inflammation. Aged $Fgl2^{-/-}$ mice develop spontaneous skin inflammation and lupus-like phenotypes with elevation of autoantibodies, highlighting the critical role of Fgl2 in regulating autoimmunity. We showed that

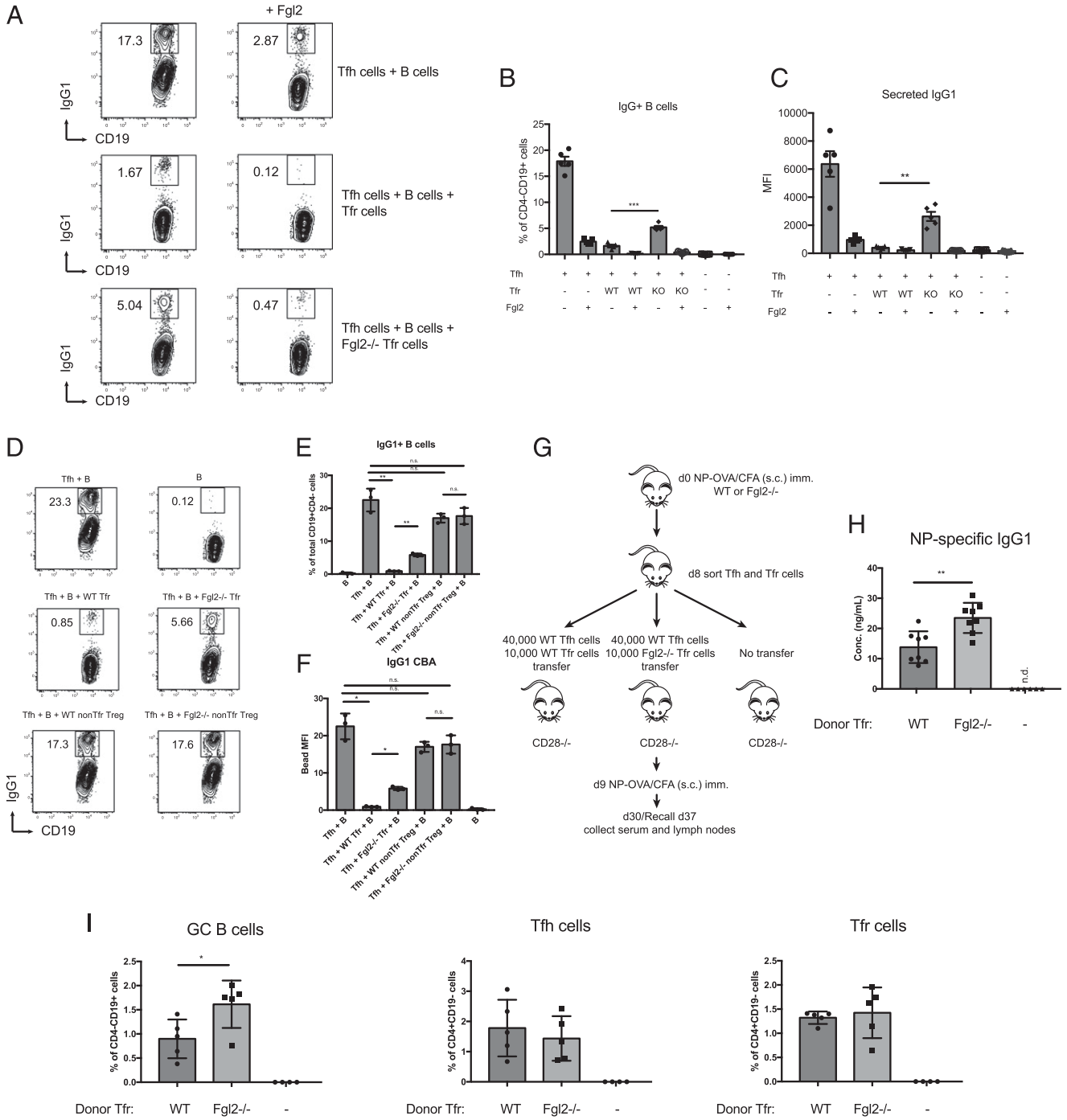

FIGURE 6. Fgl2 from TFR cells regulates Ab responses in vitro and in vivo. (**A**–**C**) In vitro coculture assay, 50,000 $Fgl2^{-/-}$-sorted total $CD19^+$ B cells from immunized mice were cocultured with 30,000 TFH cells and 3000 wild-type or $Fgl2^{-/-}$ TFR cells in the presence of soluble anti-CD3 and anti-IgM Abs. Recombinant Fgl2 was added in certain conditions. (**D**–**F**) In vitro coculture assay with the same settings as (A–C), whereas conditions with 3000 wild-type or $Fgl2^{-/-}$ non-TFR Treg cells were included. (**G**–**I**) Sorted 50,000 WT or $Fgl2^{-/-}$ $CD19^-CD4^+CXCR5^+PD1^+$ T cells (TFH + TFR cells) were transferred into $CD28^{-/-}$ mice. The mice were then immunized with NP-OVA/CFA for 14 d, and NP-specific IgG1 was detected by ELISA (H). After 30 d, recall responses were induced, and cellular composition of inguinal lymph nodes were analyzed by flow cytometry (I). The results were pooled from two to five independent experiments. All plots show the mean ± SD. $*p < 0.05$, $**p < 0.01$, $***p < 0.001$, between two groups, using Kruskal–Wallis tests, followed by post hoc Dunn tests for multiple comparisons. n.s, not significant.

Fgl2 directly acts on B cells and TFH cells and regulates Ab production and CSR, and TFR-derived Fgl2 is critical for these processes, thus demonstrating that Fgl2 is a TFR effector molecule both in vitro and in vivo.

Upon their discoveries, TFR cells were shown to express Treg-associated genes along with TFH-associated ones (19–21). Our data, based on transcriptome at the resolution of single cells through a clustering scheme, showed that TFR cells are similar to effector Treg cells, as they are in the same cluster in *t*-SNE. The finding is consistent with what was observed earlier among Treg cells (54). Our analysis, however, also took well-defined TFH cells into account. The results, therefore, demonstrate that TFR cells are still fundamentally Treg cells that express some TFH-associated genes rather than simply Treg/TFH hybrid cells.

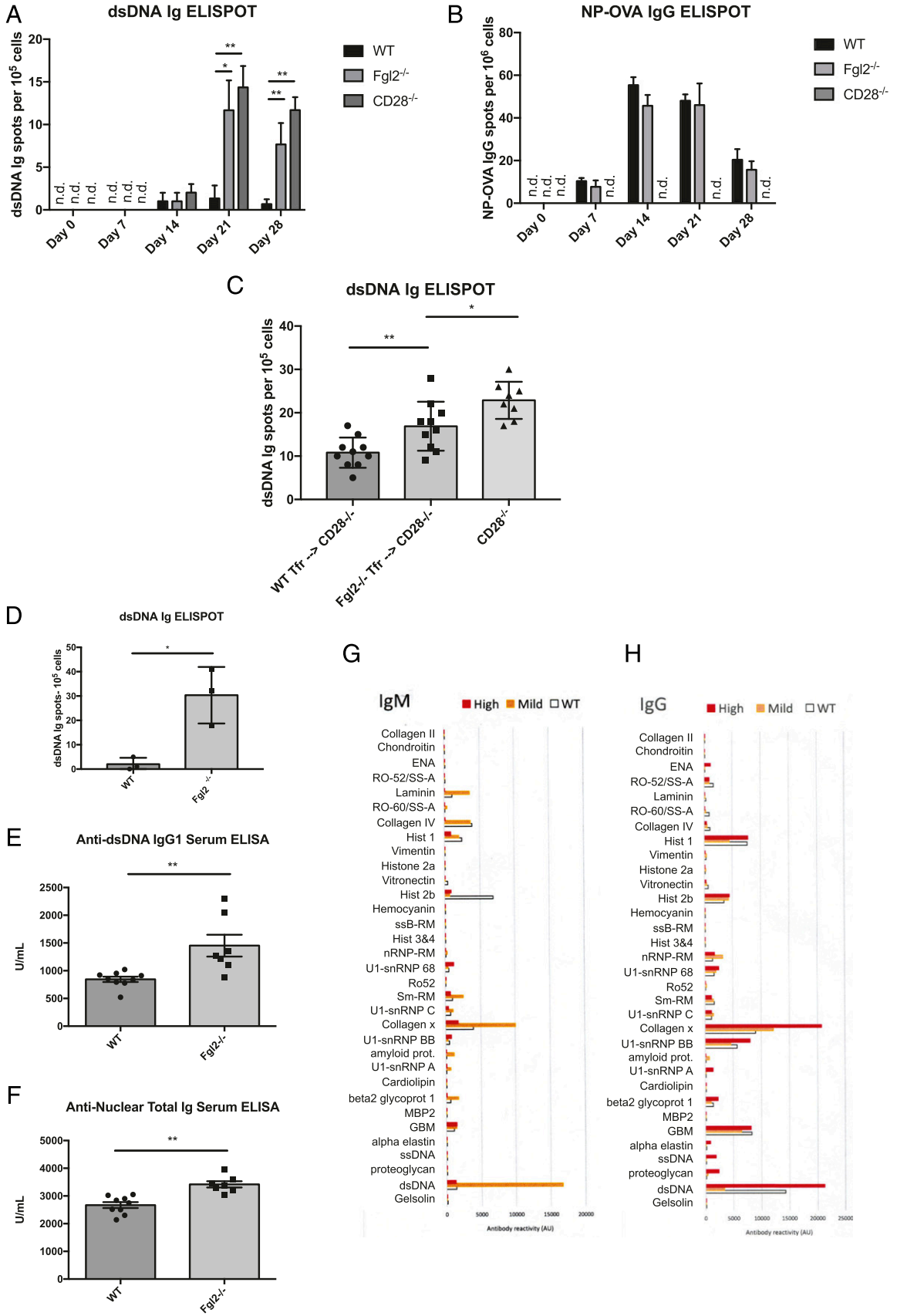

FIGURE 7. Fgl2 is important for limiting autoantibodies. (**A** and **B**) Wild-type and Fgl2$^{-/-}$ mice were immunized by NP-OVA/CFA (with additional heat-killed, dried *M. tuberculosis*). Inguinal lymph nodes were harvested at the time points indicated, and the cells were subjected to ELISPOT assay to detect dsDNA Ig and NP-OVA IgG ASCs. (**C**) Sorted 10,000 WT or Fgl2$^{-/-}$ CD19^{-}CD4^{+}CXCR5^{+}PD1^{+}Foxp3^{+} TFR cells were transferred into CD28$^{-/-}$ mice. The mice were then immunized with NP-OVA/CFA (with additional heat-killed, dried *M. tuberculosis*) for 21 d, and dsDNA Ig ASCs were detected by ELISPOT (**D**) Splenocytes from 12-mo-old wild-type and Fgl2$^{-/-}$ mice were subjected to dsDNA Ig ELISPOT. (**E** and **F**) Anti-dsDNA IgG1 and ANA in sera from 12-mo-old wild-type and Fgl2$^{-/-}$ mice were measured by ELISA. (**G** and **H**) An array of lupus IgM and *(Figure legend continues)*

A

	Aged WT (%rate)	Aged Fgl2$^{-/-}$ (%rate)
Skin-associated phenotypes (external; hairless patches to dermatitis)	0/9 (0%)	8/19 (42%)
Hyperkeratosis, dermal scarring	0/9 (0%)	5/19 (26%)
Skin infiltration of T/B cells	0/9 (0%)	3/19 (16%)
Reactive germinal centers	0/9 (0%)	3/19 (16%)
Skin infiltration of mast cells, activated macrophages	0/9 (0%)	1/19 (5%)

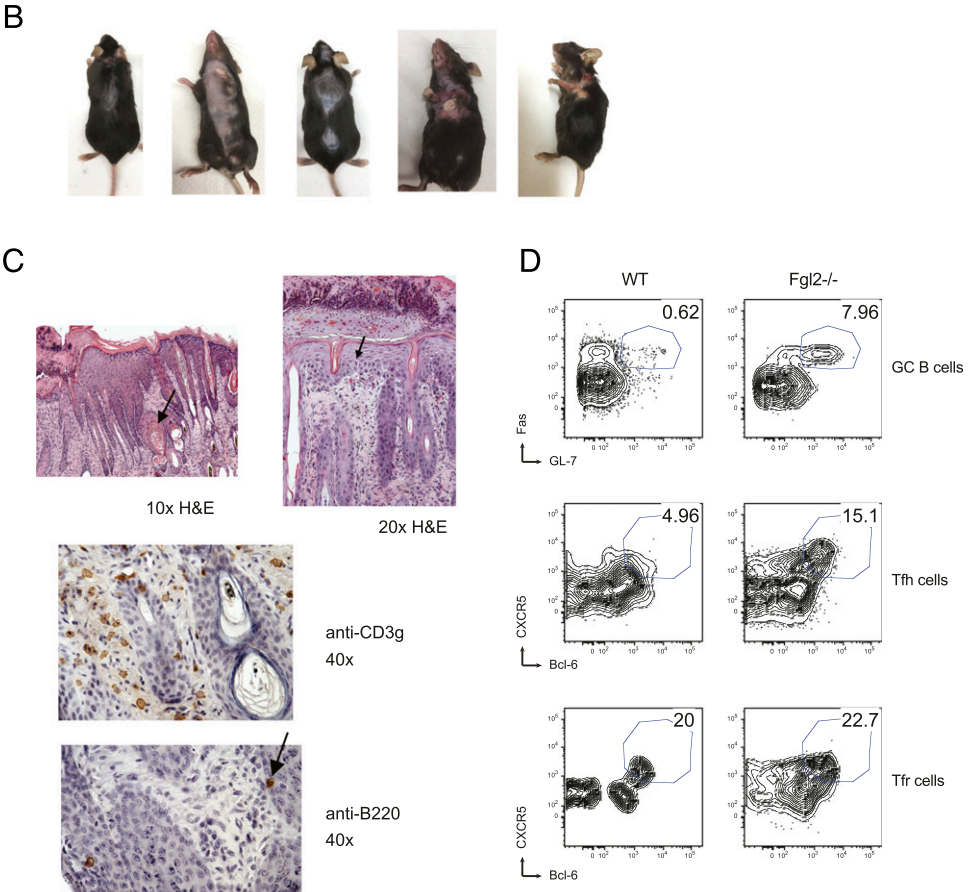

FIGURE 8. Aged Fgl2$^{-/-}$ mice developed inflammatory, lupus-like features. (**A** and **B**) A portion of aged, 12-mo-old, Fgl2$^{-/-}$ mice spontaneously developed skin disease with varied severity. (**C**) Histological analysis shows signs of surface ulceration, hyperkeratosis, elongation of rete ridges, dermal scarring, epidermolysis, follicular plugging (arrow), and basal cell discohesion (arrow). Infiltration of T cells and B cells was also observed. (**D**) Cellular composition of mice with spontaneous reactive splenic GCs showed increase in GC B cells and TFH cells. The assessment histological phenotype and its frequencies are based on one large single cohort of mice, with the numbers shown in (A), whereas representative results were shown in (B)–(D).

The suppression of type 2 Ab responses by Fgl2 was unexpected, as Fgl2 was previously shown to suppress effector Th1 and Th17, but not Th2 cells (48). However, our data also demonstrated that the effects of Fgl2 are, in fact, context and cell type dependent (Fig. 4A, Supplemental Fig. 5A). The presence of B cells, which is required for maintaining the TFH phenotype (Supplemental Fig. 5B), dictates this bias, as in the absence of B cells, we observed extensive cytokine suppression effects in non-TFH effector cells cultured in vitro. It is important to note that even though Fgl2 suppresses type 2 Ab responses directly on B cells, its effect can be exerted through TFH cells via the Fcgr2b receptor (Fig. 4B), suggesting a nuanced mechanism. Thus, it is not surprising that the contexts in which Fgl2 is expressed and the cells it acts on could lead to different effector outcomes.

On TFH cells, we have shown that Fgl2 induces *Prdm1* in an Fcgr2b-depedent fashion, and the pathway partly exerts inhibition of TFH-mediated IgG1 CSR on B cells. Expression of *Prdm1* is potentially critical at multiple levels, including antagonization of Bcl6 (7) and induction of a panel of checkpoint molecules (PD1, TIM3, LAG3, and TIGIT). It is possible that dysregulation of checkpoint molecule expression might account for some autoimmune phenotypes we observed in aged Fgl2-deficient mice. In fact, it was recently observed that germline HAVCR2 (encoding TIM3) mutations were associated with s.c. panniculitis-like T cell

IgG autoantibodies were measured in sera from 12-mo-old wild-type ($n = 6$) and Fgl2$^{-/-}$ mice ($n = 9$) using autoantigen microarray. Fgl2$^{-/-}$ mice with mild diseases ($n = 5$) had either normal histology or mild dermatitis, whereas the one with high, severe diseases ($n = 4$) had inflammation in multiple organs, including severe dermatitis, reactive changes in the spleen, ileitis, enlarged PP, and increased lymphoid clusters in lung. The results were pooled from two to three independent experiments. The autoantigen microarray results for (G) and (H) are from one independent experiment. All plots show the mean ± SD. *$p < 0.05$, **$p < 0.01$, between two groups, using Kruskal–Wallis tests, followed by post hoc Dunn tests for multiple comparisons for (A)–(C) and two-tailed unpaired Welch *t*-tests for (D)–(F). n.s, not significant.

lymphomas, with some patients developing lupus-like disease with anti-DNA Abs (55).

Although Fgl2 produced by Treg cells has been previously shown to inhibit effector T cell responses, its functions based on TFR cells have not been studied. In this study, we demonstrated the relevance of Fgl2 in TFR cells to regulate Ab responses both in vitro and in vivo. In addition, mice deficient in Fgl2, unlike total Treg-deficient mice with severe multiorgan inflammation at young age (56, 57), were generally healthy at a young age, whereas immunization led to altered isotypes against the immunized Ag. Notably, such immunization also induced local induction of autoreactive B cells producing anti-dsDNA. The phenotype was similar to that observed in TFR-deficient mice (22, 23) in which alterations in humoral responses against foreign Ags were subtle, whereas the mice only developed autoimmunity at an older age or upon induction. To what extent the spontaneous development of autoimmune phenotype, particularly skin inflammation, in aged Fgl2-deficient mice is dependent on Fgl2 from TFR cells, however, is still not known. The observation, nonetheless, collectively supports the relevance of Fgl2 as a key regulator of tissue inflammation and autoimmunity; however, what needs to be resolved is the relative roles that Fgl2 plays in inducing autoimmunity when produced by Tregs versus TFR cells.

Recent studies have implicated TFR cells in limiting autoimmunity (22, 23). Our observations that NP-OVA immunization was sufficient to induce transient and local induction of autoreactive B cells in Fgl2-deficient mice. Furthermore, the Fgl2-deficient mice spontaneously developed dermatitis and multiple types of autoantibodies against lupus-associated autoantigens with age suggested that Fgl2 is an effector molecule used by TFR cells to control autoreactive B cells. TFR cells might directly interact with autoreactive B cells themselves as their TCR repertoire is skewed toward self-antigen (58). Our data, in addition, show that Fgl2 is only able to limit B cell survival and proliferation in the absence of cognate TFH help (Supplemental Fig. 3E) or another costimulatory pathway like TLR4 by LPS stimulation (Supplemental Fig. 3B). This observation implies that through Fgl2, TFR cells might specifically target autoreactive B cells because of their lack of help from cognate TFH cells. Moreover, dysregulation in costimulatory pathways such as TLR pathways that leads to autoreactive B cell dysregulation (59, 60) might be partially due to their resistance to TFR suppression.

The presence of autoantibodies against lupus-associated autoantigens in aged Fgl2$^{-/-}$ mice lead to the hypothesis that Fgl2 may be a relevant molecule in lupus and/or other humoral autoimmune diseases like Sjogren syndrome. In fact, mice with Fcgr2b deficiency develop a spontaneous lupus-like disease with high-titer autoantibodies and B cells from the mice can lead to the development of lupus-like disease (61). Furthermore, polymorphisms in both low-affinity Fc receptors known to bind to Fgl2 have been shown to be associated with susceptibility to systemic lupus erythematosus in humans (62–66). These studies not only underscore the role of these Fc receptors but may also suggest that the effects are partly due to loss of Fgl2 signaling.

Fgl2$^{-/-}$ mice have been reported previously to develop glomerulonephritis, which we did not observe in our cohort (31). However, we were able to see spontaneous GC cell phenotype in spleens in a small portion of the observed group. This suggests that additional environmental factors, including possible variation in the microbiome in our housing facility, likely modulate disease. As we hypothesize that the phenotypes observed with age were due to the accumulated insults over the lifespan, the variability in the frequency and the underlying natures of such insults, like host–microbiome interaction, might result in manifestation of different clinical phenotypes in Fgl2-deficient mice.

Taken together, our work uncovered Fgl2 as a TFR cell effector molecule that directly acts on B cells and TFH cells. To our knowledge, this finding provides a novel path for targeting Ab responses by modulating TFR effector function, which could potentially be useful for vaccine development and, through supplementation, for treating systemic autoimmune diseases.

Acknowledgments

We thank Deneen Kozoriz (Evergrande Center) for cell sorting, Mary Collins for advice and editing of the manuscript, and Michelle Weinstein for editing of the manuscript.

Disclosures

V.K.K. is a member of the scientific advisory boards for Compass Therapeutics and Tizona Therapeutics, which have interests in cancer immunotherapy. V.K.K. has an ownership interest in and is a member of the scientific advisory board for Tizona Therapeutics. V.K.K. is a co-founder of and has an ownership interest in Celsius Therapeutics. V.K.K.'s interests were reviewed and managed by the Brigham and Women's Hospital and Partners Healthcare in accordance with their conflict of interest policies. V.K.K. is a named inventor on patents related to TIM3 and TIGIT. The other authors have no financial conflicts of interest.

References

1. De Silva, N. S., and U. Klein. 2015. Dynamics of B cells in germinal centres. *Nat. Rev. Immunol.* 15: 137–148.
2. Victora, G. D., and M. C. Nussenzweig. 2012. Germinal centers. *Annu. Rev. Immunol.* 30: 429–457.
3. Crotty, S. 2011. Follicular helper CD4 T cells (TFH). *Annu. Rev. Immunol.* 29: 621–663.
4. Schaerli, P., K. Willimann, A. B. Lang, M. Lipp, P. Loetscher, and B. Moser. 2000. CXC chemokine receptor 5 expression defines follicular homing T cells with B cell helper function. *J. Exp. Med.* 192: 1553–1562.
5. Kim, C. H., L. S. Rott, I. Clark-Lewis, D. J. Campbell, L. Wu, and E. C. Butcher. 2001. Subspecialization of CXCR5$^+$ T cells: B helper activity is focused in a germinal center-localized subset of CXCR5$^+$ T cells. *J. Exp. Med.* 193: 1373–1381.
6. Breitfeld, D., L. Ohl, E. Kremmer, J. Ellwart, F. Sallusto, M. Lipp, and R. Förster. 2000. Follicular B helper T cells express CXC chemokine receptor 5, localize to B cell follicles, and support immunoglobulin production. *J. Exp. Med.* 192: 1545–1552.
7. Johnston, R. J., A. C. Poholek, D. DiToro, I. Yusuf, D. Eto, B. Barnett, A. L. Dent, J. Craft, and S. Crotty. 2009. Bcl6 and Blimp-1 are reciprocal and antagonistic regulators of T follicular helper cell differentiation. *Science* 325: 1006–1010.
8. Nurieva, R. I., Y. Chung, G. J. Martinez, X. O. Yang, S. Tanaka, T. D. Matskevitch, Y. H. Wang, and C. Dong. 2009. Bcl6 mediates the development of T follicular helper cells. *Science* 325: 1001–1005.
9. Yu, D., S. Rao, L. M. Tsai, S. K. Lee, Y. He, E. L. Sutcliffe, M. Srivastava, M. Linterman, L. Zheng, N. Simpson, et al. 2009. The transcriptional repressor Bcl-6 directs T follicular helper cell lineage commitment. *Immunity* 31: 457–468.
10. Bauquet, A. T., H. Jin, A. M. Paterson, M. Mitsdoerffer, I. C. Ho, A. H. Sharpe, and V. K. Kuchroo. 2009. The costimulatory molecule ICOS regulates the expression of c-Maf and IL-21 in the development of follicular T helper cells and TH-17 cells. *Nat. Immunol.* 10: 167–175.
11. Liu, X., X. Chen, B. Zhong, A. Wang, X. Wang, F. Chu, R. I. Nurieva, X. Yan, P. Chen, L. G. van der Flier, et al. 2014. Transcription factor achaete-scute homologue 2 initiates follicular T-helper-cell development. *Nature* 507: 513–518.
12. McAdam, A. J., R. J. Greenwald, M. A. Levin, T. Chernova, N. Malenkovich, V. Ling, G. J. Freeman, and A. H. Sharpe. 2001. ICOS is critical for CD40-mediated antibody class switching. *Nature* 409: 102–105.
13. Ozaki, K., R. Spolski, C. G. Feng, C. F. Qi, J. Cheng, A. Sher, H. C. Morse, III, C. Liu, P. L. Schwartzberg, and W. J. Leonard. 2002. A critical role for IL-21 in regulating immunoglobulin production. *Science* 298: 1630–1634.
14. Nurieva, R. I., Y. Chung, D. Hwang, X. O. Yang, H. S. Kang, L. Ma, Y. H. Wang, S. S. Watowich, A. M. Jetten, Q. Tian, and C. Dong. 2008. Generation of T follicular helper cells is mediated by interleukin-21 but independent of T helper 1, 2, or 17 cell lineages. *Immunity* 29: 138–149.
15. Reinhardt, R. L., H. E. Liang, and R. M. Locksley. 2009. Cytokine-secreting follicular T cells shape the antibody repertoire. *Nat. Immunol.* 10: 385–393.
16. Yusuf, I., R. Kageyama, L. Monticelli, R. J. Johnston, D. Ditoro, K. Hansen, B. Barnett, and S. Crotty. 2010. Germinal center T follicular helper cell IL-4 production is dependent on signaling lymphocytic activation molecule receptor (CD150). *J. Immunol.* 185: 190–202.

17. Choi, Y. S., R. Kageyama, D. Eto, T. C. Escobar, R. J. Johnston, L. Monticelli, C. Lao, and S. Crotty. 2011. ICOS receptor instructs T follicular helper cell versus effector cell differentiation via induction of the transcriptional repressor Bcl6. *Immunity* 34: 932–946.
18. Xu, H., X. Li, D. Liu, J. Li, X. Zhang, X. Chen, S. Hou, L. Peng, C. Xu, W. Liu, et al. 2013. Follicular T-helper cell recruitment governed by bystander B cells and ICOS-driven motility. *Nature* 496: 523–527.
19. Linterman, M. A., W. Pierson, S. K. Lee, A. Kallies, S. Kawamoto, T. F. Rayner, M. Srivastava, D. P. Divekar, L. Beaton, J. J. Hogan, et al. 2011. Foxp3$^+$ follicular regulatory T cells control the germinal center response. *Nat. Med.* 17: 975–982.
20. Chung, Y., S. Tanaka, F. Chu, R. I. Nurieva, G. J. Martinez, S. Rawal, Y. H. Wang, H. Lim, J. M. Reynolds, X. H. Zhou, et al. 2011. Follicular regulatory T cells expressing Foxp3 and Bcl-6 suppress germinal center reactions. *Nat. Med.* 17: 983–988.
21. Wollenberg, I., A. Agua-Doce, A. Hernández, C. Almeida, V. G. Oliveira, J. Faro, and L. Graca. 2011. Regulation of the germinal center reaction by Foxp3$^+$ follicular regulatory T cells. *J. Immunol.* 187: 4553–4560.
22. Botta, D., M. J. Fuller, T. T. Marquez-Lago, H. Bachus, J. E. Bradley, A. S. Weinmann, A. J. Zajac, T. D. Randall, F. E. Lund, B. León, and A. Ballesteros-Tato. 2017. Dynamic regulation of T follicular regulatory cell responses by interleukin 2 during influenza infection. *Nat. Immunol.* 18: 1249–1260.
23. Fu, W., X. Liu, X. Lin, H. Feng, L. Sun, S. Li, H. Chen, H. Tang, L. Lu, W. Jin, and C. Dong. 2018. Deficiency in T follicular regulatory cells promotes autoimmunity. *J. Exp. Med.* 215: 815–825.
24. Martins, G. A., L. Cimmino, M. Shapiro-Shelef, M. Szabolcs, A. Herron, E. Magnusdottir, and K. Calame. 2006. Transcriptional repressor Blimp-1 regulates T cell homeostasis and function. *Nat. Immunol.* 7: 457–465.
25. Cretney, E., A. Xin, W. Shi, M. Minnich, F. Masson, M. Miasari, G. T. Belz, G. K. Smyth, M. Busslinger, S. L. Nutt, and A. Kallies. 2011. The transcription factors Blimp-1 and IRF4 jointly control the differentiation and function of effector regulatory T cells. *Nat. Immunol.* 12: 304–311.
26. Cretney, E., A. Kallies, and S. L. Nutt. 2013. Differentiation and function of Foxp3$^+$ effector regulatory T cells. *Trends Immunol.* 34: 74–80.
27. Sage, P. T., N. Ron-Harel, V. R. Juneja, D. R. Sen, S. Maleri, W. Sungnak, V. K. Kuchroo, W. N. Haining, N. Chevrier, M. Haigis, and A. H. Sharpe. 2016. Suppression by T_{FR} cells leads to durable and selective inhibition of B cell effector function. *Nat. Immunol.* 17: 1436–1446.
28. Sage, P. T., A. M. Paterson, S. B. Lovitch, and A. H. Sharpe. 2014. The coinhibitory receptor CTLA-4 controls B cell responses by modulating T follicular helper, T follicular regulatory, and T regulatory cells. *Immunity* 41: 1026–1039.
29. Wing, J. B., W. Ise, T. Kurosaki, and S. Sakaguchi. 2014. Regulatory T cells control antigen-specific expansion of Tfh cell number and humoral immune responses via the coreceptor CTLA-4. *Immunity* 41: 1013–1025.
30. Bettelli, E., Y. Carrier, W. Gao, T. Korn, T. B. Strom, M. Oukka, H. L. Weiner, and V. K. Kuchroo. 2006. Reciprocal developmental pathways for the generation of pathogenic effector TH17 and regulatory T cells. *Nature* 441: 235–238.
31. Shalev, I., H. Liu, C. Koscik, A. Bartczak, M. Javadi, K. M. Wong, A. Maknojia, W. He, M. F. Liu, J. Diao, et al. 2008. Targeted deletion of fgl2 leads to impaired regulatory T cell activity and development of autoimmune glomerulonephritis. *J. Immunol.* 180: 249–260.
32. Sage, P. T., L. M. Francisco, C. V. Carman, and A. H. Sharpe. 2013. The receptor PD-1 controls follicular regulatory T cells in the lymph nodes and blood. *Nat. Immunol.* 14: 152–161.
33. Trombetta, J. J., D. Gennert, D. Lu, R. Satija, A. K. Shalek, and A. Regev. 2014. Preparation of single-cell RNA-seq libraries for next generation sequencing. *Curr. Protoc. Mol. Biol.* 107: 4.22.1–4.22.17.
34. Gaublomme, J. T., N. Yosef, Y. Lee, R. S. Gertner, L. V. Yang, C. Wu, P. P. Pandolfi, T. Mak, R. Satija, A. K. Shalek, et al. 2015. Single-cell genomics unveils critical regulators of Th17 cell pathogenicity. *Cell* 163: 1400–1412.
35. Sage, P. T., and A. H. Sharpe. 2015. In vitro assay to sensitively measure T(FR) suppressive capacity and T(FH) stimulation of B cell responses. *Methods Mol. Biol.* 1291: 151–160.
36. Sage, P. T., D. Alvarez, J. Godec, U. H. von Andrian, and A. H. Sharpe. 2014. Circulating T follicular regulatory and helper cells have memory-like properties. *J. Clin. Invest.* 124: 5191–5204.
37. Quintana, F. J., P. H. Hagedorn, G. Elizur, Y. Merbl, E. Domany, and I. R. Cohen. 2004. Functional immunomics: microarray analysis of IgG autoantibody repertoires predicts the future response of mice to induced diabetes. *Proc. Natl. Acad. Sci. USA* 101(Suppl. 2): 14615–14621.
38. Li, Q. Z., C. Xie, T. Wu, M. Mackay, C. Aranow, C. Putterman, and C. Mohan. 2005. Identification of autoantibody clusters that best predict lupus disease activity using glomerular proteome arrays. [Published erratum appears in 2006 *J. Clin. Invest.* 116: 548.] *J. Clin. Invest.* 115: 3428–3439.
39. Wu, H. Y., F. J. Quintana, and H. L. Weiner. 2008. Nasal anti-CD3 antibody ameliorates lupus by inducing an IL-10-secreting CD4$^+$CD25$^-$LAP$^+$ regulatory T cell and is associated with down-regulation of IL-17$^+$CD4$^+$ICOS$^+$CXCR5$^+$ follicular helper T cells. *J. Immunol.* 181: 6038–6050.
40. Butler, A., P. Hoffman, P. Smibert, E. Papalexi, and R. Satija. 2018. Integrating single-cell transcriptomic data across different conditions, technologies, and species. *Nat. Biotechnol.* 36: 411–420.
41. Kim, D., G. Pertea, C. Trapnell, H. Pimentel, R. Kelley, and S. L. Salzberg. 2013. TopHat2: accurate alignment of transcriptomes in the presence of insertions, deletions and gene fusions. *Genome Biol.* 14: R36.
42. Liao, Y., G. K. Smyth, and W. Shi. 2014. featureCounts: an efficient general purpose program for assigning sequence reads to genomic features. *Bioinformatics* 30: 923–930.
43. Love, M. I., W. Huber, and S. Anders. 2014. Moderated estimation of fold change and dispersion for RNA-seq data with DESeq2. *Genome Biol.* 15: 550.
44. Wagner, A., A. Regev, and N. Yosef. 2016. Revealing the vectors of cellular identity with single-cell genomics. *Nat. Biotechnol.* 34: 1145–1160.
45. Waltman, L., and N. J. van Eck. 2013. A smart local moving algorithm for large-scale modularity-based community detection. *Eur. Phys. J. B* 86: 471.
46. Cho, S. H., A. L. Raybuck, J. Blagih, E. Kemboi, V. H. Haase, R. G. Jones, and M. R. Boothby. 2019. Hypoxia-inducible factors in CD4$^+$ T cells promote metabolism, switch cytokine secretion, and T cell help in humoral immunity. *Proc. Natl. Acad. Sci. USA* 116: 8975–8984.
47. Dang, E. V., J. Barbi, H. Y. Yang, D. Jinasena, H. Yu, Y. Zheng, Z. Bordman, J. Fu, Y. Kim, H. R. Yen, et al. 2011. Control of T(H)17/T(reg) balance by hypoxia-inducible factor 1. *Cell* 146: 772–784.
48. Joller, N., E. Lozano, P. R. Burkett, B. Patel, S. Xiao, C. Zhu, J. Xia, T. G. Tan, E. Sefik, V. Yajnik, et al. 2014. Treg cells expressing the coinhibitory molecule TIGIT selectively inhibit proinflammatory Th1 and Th17 cell responses. *Immunity* 40: 569–581.
49. Liu, H., I. Shalev, J. Manuel, W. He, E. Leung, J. Crookshank, M. F. Liu, J. Diao, M. Cattral, D. A. Clark, et al. 2008. The FGL2-FcgammaRIIB pathway: a novel mechanism leading to immunosuppression. *Eur. J. Immunol.* 38: 3114–3126.
50. Liu, H., L. Zhang, M. Cybulsky, R. Gorczynski, J. Crookshank, J. Manuel, D. Grant, and G. Levy. 2006. Identification of the receptor for FGL2 and implications for susceptibility to mouse hepatitis virus (MHV-3)-induced fulminant hepatitis. *Adv. Exp. Med. Biol.* 581: 421–425.
51. Victora, G. D., T. A. Schwickert, D. R. Fooksman, A. O. Kamphorst, M. Meyer-Hermann, M. L. Dustin, and M. C. Nussenzweig. 2010. Germinal center dynamics revealed by multiphoton microscopy with a photoactivatable fluorescent reporter. *Cell* 143: 592–605.
52. Shin, H., S. D. Blackburn, A. M. Intlekofer, C. Kao, J. M. Angelosanto, S. L. Reiner, and E. J. Wherry. 2009. A role for the transcriptional repressor Blimp-1 in CD8$^+$ T cell exhaustion during chronic viral infection. *Immunity* 31: 309–320.
53. Chihara, N., A. Madi, T. Kondo, H. Zhang, N. Acharya, M. Singer, J. Nyman, N. D. Marjanovic, M. S. Kowalczyk, C. Wang, et al. 2018. Induction and transcriptional regulation of the co-inhibitory gene module in T cells. *Nature* 558: 454–459.
54. Zemmour, D., R. Zilionis, E. Kiner, A. M. Klein, D. Mathis, and C. Benoist. 2018. Single-cell gene expression reveals a landscape of regulatory T cell phenotypes shaped by the TCR. [Published erratum appears in 2018 *Nat. Immunol.* 19: 645.] *Nat. Immunol.* 19: 291–301.
55. Gayden, T., F. E. Sepulveda, D.-A. Khuong-Quang, J. Pratt, E. T. Valera, A. Garrigue, S. Kelso, F. Sicheri, L. G. Mikael, N. Hamel, et al. 2018. Germline HAVCR2 mutations altering TIM-3 characterize subcutaneous panniculitis-like T cell lymphomas with hemophagocytic lymphohistiocytic syndrome. [Published erratum appears in 2019 *Nat. Genet.* 51: 196.] *Nat. Genet.* 50: 1650–1657.
56. Godfrey, V. L., J. E. Wilkinson, E. M. Rinchik, and L. B. Russell. 1991. Fatal lymphoreticular disease in the scurfy (sf) mouse requires T cells that mature in a sf thymic environment: potential model for thymic education. *Proc. Natl. Acad. Sci. USA* 88: 5528–5532.
57. Hadaschik, E. N., X. Wei, H. Leiss, B. Heckmann, B. Niederreiter, G. Steiner, W. Ulrich, A. H. Enk, J. S. Smolen, and G. H. Stummvoll. 2015. Regulatory T cell-deficient scurfy mice develop systemic autoimmune features resembling lupus-like disease. *Arthritis Res. Ther.* 17: 35.
58. Maceiras, A. R., S. C. P. Almeida, E. Mariotti-Ferrandiz, W. Chaara, F. Jebbawi, A. Six, S. Hori, D. Klatzmann, J. Faro, and L. Graca. 2017. T follicular helper and T follicular regulatory cells have different TCR specificity. *Nat. Commun.* 8: 15067.
59. Barrat, F. J., T. Meeker, J. Gregorio, J. H. Chan, S. Uematsu, S. Akira, B. Chang, O. Duramad, and R. L. Coffman. 2005. Nucleic acids of mammalian origin can act as endogenous ligands for Toll-like receptors and may promote systemic lupus erythematosus. *J. Exp. Med.* 202: 1131–1139.
60. Christensen, S. R., J. Shupe, K. Nickerson, M. Kashgarian, R. A. Flavell, and M. J. Shlomchik. 2006. Toll-like receptor 7 and TLR9 dictate autoantibody specificity and have opposing inflammatory and regulatory roles in a murine model of lupus. *Immunity* 25: 417–428.
61. Bolland, S., and J. V. Ravetch. 2000. Spontaneous autoimmune disease in Fc(gamma)RIIB-deficient mice results from strain-specific epistasis. *Immunity* 13: 277–285.
62. Willcocks, L. C., E. J. Carr, H. A. Niederer, T. F. Rayner, T. N. Williams, W. Yang, J. A. Scott, B. C. Urban, N. Peshu, T. J. Vyse, et al. 2010. A defunctioning polymorphism in FCGR2B is associated with protection against malaria but susceptibility to systemic lupus erythematosus. *Proc. Natl. Acad. Sci. USA* 107: 7881–7885.
63. Chen, J. Y., C. M. Wang, C. C. Ma, S. F. Luo, J. C. Edberg, R. P. Kimberly, and J. Wu. 2006. Association of a transmembrane polymorphism of Fcgamma receptor IIb (FCGR2B) with systemic lupus erythematosus in Taiwanese patients. *Arthritis Rheum.* 54: 3908–3917.
64. Chu, Z. T., N. Tsuchiya, C. Kyogoku, J. Ohashi, Y. P. Qian, S. B. Xu, C. Z. Mao, J. Y. Chu, and K. Tokunaga. 2004. Association of Fcgamma receptor IIb polymorphism with susceptibility to systemic lupus erythematosus in Chinese: a common susceptibility gene in the Asian populations. *Tissue Antigens* 63: 21–27.
65. Kyogoku, C., H. M. Dijstelbloem, N. Tsuchiya, Y. Hatta, H. Kato, A. Yamaguchi, T. Fukazawa, M. D. Jansen, H. Hashimoto, J. G. van de Winkel, et al. 2002. Fcgamma receptor gene polymorphisms in Japanese patients with systemic lupus erythematosus: contribution of FCGR2B to genetic susceptibility. *Arthritis Rheum.* 46: 1242–1254.
66. Siriboonrit, U., N. Tsuchiya, M. Sirikong, C. Kyogoku, S. Bejrachandra, P. Suthipinittharm, K. Luangtrakool, D. Srinak, R. Thongpradit, K. Fujiwara, et al. 2003. Association of Fcgamma receptor IIb and IIIb polymorphisms with susceptibility to systemic lupus erythematosus in Thais. *Tissue Antigens* 61: 374–383.